Semi-Autonomous UAV for Surveillance and Emergency Response (SAUSER)

Final Design Review

ISYE 4803

Aeronautics Senior Design Project

Spring 2021

Due date: April 28, 2021

Faculty Advisor: Dr. Adeel Khalid

Group Members:

Ryan Foster – Project Manager, Simulation Engineering Lead

Arshdeep Sandhu – Project Coordinator, Engineering Manager

Kenneth Jones – Design & Manufacturing Lead

Table of Contents

List of Figures

List of Tables

Executive Summary

The SAUSER is a drone system that can provide aerial footage of traffic accidents and other emergency situations. The drone system has mounting docks that can be mounted on traffic lights to allow for rapid deployment. The mounting docks also function as charging stations.

Literature review was performed to determine the current status of drones in law enforcement. Review was done on both the technological capabilities of drones as well as the legal requirements for drone operation by law enforcement.

Concept alternatives were considered to determine the best solution for this problem. A quadcopter with no landing gear was chosen as the best solution to the problem. Design requirements, performance metrics, and estimated budget were developed.

Off the shelf electronics were selected to provide the necessary thrust, charging, video feed, and wireless capabilities necessary for the remote operation of the drones from a 911 dispatching station. Sizing calculations were performed to determine the takeoff weight of the drone. Blade Element Momentum Theory analysis was performed to determine if the blades could provide proper thrust.

Computational Fluid Dynamics and Finite Element Analysis was performed to determine if the drone would experience mechanical failure during the lifecycle of the project. Hand calculations were done to verify the validity of these results.

Finally, an economic analysis was performed to determine if the drone meet the budgetary requirements established in the previous sections. It was also done to determine the total cost of the system over a ten-year period.

Chapter 1: Introduction

1.1: Introduction

The objective of this project was to perform a concept design of a drone optimized for first response in emergency traffic situations. This drone can provide rapid information gathering to enable first responders to decide on a further course of action. The primary advantage this drone has over other emergency response drones is that its design is optimized for traffic situations. This specialization allows the drone to be implemented at a lower cost point than other similar options.

1.2: System Overview

The Semi-Autonomous UAV for Surveillance and Emergency Response (SAUSER) system utilizes a local area network that allows drone pilots in 911 centers to control the drones in emergency situations. From the command center, the operator is able to dispatch a drone using the provided software to provide a third person, omniscient, view of traffic stops, accidents, and other critical level emergency situations. Camera footage is relayed using a local area network supported by the drone docking stations at the intersections. The footage is then archived for litigation and insurance purposes for the public.

The major components consist of the chassis, battery, flight controller, motors, and the intersection-based docking station. The chassis is the metal body that protects the components from the elements. The body will be watertight to protect the electrical components. The battery is a rechargeable lithium-ion battery that supplies the drone enough energy to complete its designated mission with a reasonable factor of safety. To keep the drone free of human interaction, it is charged using wireless charging at the dock. A wireless charging coil is located under the battery and inside the chassis to provide easy charging.

The flight controller is the control module for the drone. Pilots control the drone from their workstations through Wi-Fi network, and the flight controller on the drone receives the commands. GPS information, drone diagnostics, and other pertinent data is gathered by the flight controller and sent using the telemetry radio. A video transmitter sends a live video feed from the

drone to the pilot for guidance and surveillance. The pilot also has pan and rotate ability using the gimbal onboard the drone.

Brushless motors are used in the rotor system for propulsion. The brushless motors was selected to provide for water resistance, low noise, and high speeds. Being a quadcopter design, this drone utilizes four brushless motors, four electronic speed controllers (ESC), and four propellors.

At the intersection, there is a dock for the drone to return to. The dock needs access to internet data cables and power. These should be easy to access in major intersections as they already have the access to power for traffic lights and speed cameras. The dock acts as a landing pad for the drone and as a charging station. The dock has the wireless charger for the drone's battery. The dock also operates as a wireless access point to send the video feed and telemetry data over Wi-Fi. Docking station is mounted on traffic light poles or telephone poles to prevent potential vandalization or theft. Figure 1 is a system block diagram which presents these components in a visual format.

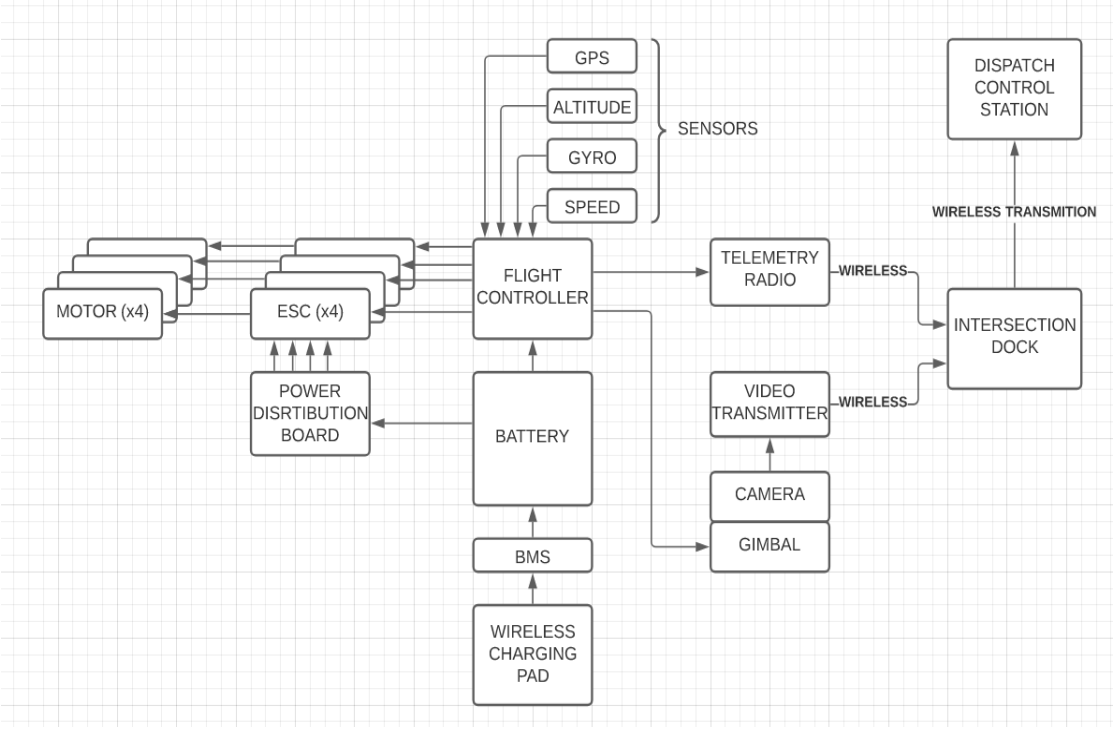

Figure 1: System block diagram for the SAUSER system.

Chapter 2: Literature Review

Drones are being introduced for a variety of first response applications including search and rescue, crime prevention, and emergency disaster response.[1] Lemayian and Mamamreh (2019) describe the benefits of using unmanned drones for rapid emergency response.[2] Drones allow for first responders to quickly assess the situation and determine what additional personnel and equipment is necessary.[2] Drones can accomplish this task much quicker than land vehicles.[2] Rizwan et al. (2019) describe a system that uses a Virtual Reality (VR) headset to allow the operation of the drone to view a camera feed from the drone.[3] These drones could also be used to map out the operational areas as described by Kucharczyk and Hugenholtz (2019).[4] Saha et al. describe a system to allow these drones to have the option of being either autonomous or remotely operated by a human controller.[5]

There already are commercially available drones designed for emergency responses, such as the Viper Drones DJI Matrice M200. This drone is designed for "multiple applications – power line inspection, search and rescue, wind turbine inspection, facilities inspection, firefighting, construction site mapping and more."[6] The SAUSER system is instead designed to handle one single application: emergency response for traffic emergencies. This allows the design to be optimized for this specific use. This specificity allows the drone to be more efficient and economical at a large scale.

A drone utilized by law enforcement can raise legal issues. The Fourth Amendment to the U.S. Constitution states:

> The right of the people to be secure in their persons, houses, papers, and effects, against unreasonable searches and seizures, shall not be violated, and no Warrants shall issue, but

---

1 Karsten and West, "How emergency responders are using drones to save lives." https://www.brookings.edu/blog/techtank/2018/12/04/how-emergency-responders-are-using-drones-to-save-lives/

2 Lemayian and Mamamreh, "First Responder Drones for Critical Situation Management." Innovations in Intelligent Systems and Applications Conference. Izmir: IEEE.

3 Rizwan et al., "Quadcopter-Based Rapid Response First-Aid Unit with Live Video Monitoring." *Drones* 37.

4 Kucharczyk and Hugenholtz, "Pre-disaster mapping with drones: an urban case study in Victoria, British Columbia, Canada." *Natural Hazards & Earth System Sciences* 2039-2051.

5 Saha et al., "A low cost fully autonomous GPS (Global Positioning System) based Quad copter for disaster management." *8th Annual Computing and Communication Workshop and Conference.* Las Vega: IEEE. 654-660.

6 Viper Drones, "DJI Matrice M200." https://viper-drones.shop/product/dji-matrice-m200/

upon probable cause, supported by Oath or affirmation, and particularly describing the place to be searched, and the persons or things to be seized.[7]

In *California v. Ciraolo*, the U.S. Supreme Court addressed the use of aerial surveillance by law enforcement.[8] In this case, the Supreme Court stated that the Fourth Amendment allows for surveillance by a fixed wing aircraft in public airspace.[8] A helicopter flying 400 feet above the ground was also confirmed by the Supreme Court in *Florida v. Riley*.[8] However, other cases have established that the aerial surveillance must be sufficiently unobtrusive to comply with the Fourth Amendment.[8] According to Porter (2015), these cases and others establish that there are two conditions necessary for aerial surveillance to be Constitutional: the aerial observation must be in public airspace and must be relatively unobtrusive.[8] An article written by Jorgensen & Salberg, LLP, is in agreeance with these conclusions.[9]

Law enforcement's use of drones is also affected by state laws. Thirteen states have passed laws banning law enforcement agencies from conducting warrantless surveillance with drones, however, only one state (Iowa) has banned the use of drones for traffic enforcement.[10] Therefore, it is the opinion of the Kennesaw State University engineering design team that this project currently will not require additional legislation to be viable in majority of the nation. However, according to Smith, drone regulations are constantly shifting and often change on a state-by-state basis.[11]

It was decided to produce the rotor blades out of carbon fiber-reinforced composites (CRFCs). Material properties of these composites were obtained from Hexcel, a manufacturer of CRFCs.[12] 7075-T6 aluminum was selected for the body and arms of the drone. The material properties for the structure and body of the drone were obtained from the SOLIDWORKS

---

[7] U.S. Constitution, https://constitution.congress.gov/constitution/
[8] Porter, "Law Enforcement's Use of Weaponized Drones: Today and Tomorrow." *Saint Louis University Law Journal* 351-370.
[9] Jorgensen & Salberg, LLP, "Can Police use Drones for Surveillance?" https://jslawgroup.com/can-police-use-drones-surveillance/
[10] Michel, "Local and State Drone Laws" https://dronecenter.bard.edu/projects/other-projects/state-and-local-drone-laws/
[11] Smith, "Regulating Law Enforcement's Use of Drones: The Need for State Legislation." *Harvard Journal on Legislation* 423-454.
[12] Hexcel, "HexTow AS4 Carbon Fiber Product Data Sheet." https://www.hexcel.com/user_area/content_media/raw/AS4_HexTow_DataSheet.pdf

material library. These material properties are obtained from ASM International.[13] This source provided the static and fatigue stress responses needed to not only do the finite element analysis, but also the manual hand calculations used to verify the results of the finite element analysis.

To perform an economic analysis, the cost of machining was estimated using custompart.net.[14] Cost of power was estimated using data from the United States Bureau of Labor Statistics.[15] This was incorporated with the parts cost to determine the cost of manufacturing the drone. The drone system will also require digital infrastructure to support a system of dispatchers. Server costs were estimated by using a quote from Rackspace Technology.[16] The drone system will also require drone operators. The cost of hiring drone operators was estimated by using the average drone operator salary in the United States from Ziprecruiter.com.[17] The drone operator salary was converted to a total cost of hiring drone operators using data from the United States Small Business Administration.[18] All this information was used to determine if the project could be accomplished within the budget.

[13] Dassault, SOLIDWORKS Material Library
[14] Custompart.net, "Die Casting Cost Estimator." https://www.custompartnet.com/estimate/die-casting/
[15] United States Bureau of Labor Statistics, "Average Energy Prices." https://www.bls.gov/regions/midwest/data/AverageEnergyPrices_SelectedAreas_Table.htm
[16] Rackspace Technology, "Cloud Server Pricing." https://www.rackspace.com/openstack/public/servers/pricing
[17] Ziprecruiter.com, "Drone Operator Annual Salary." https://www.ziprecruiter.com/Salaries/Drone-Operator-Salary
[18] United States Small Business Administration, "How Much Does an Employee Cost You?" https://www.sba.gov/blog/how-much-does-employee-cost-you

Chapter 3: Design Approach and Methodology

3.1 Problem Solving Approach

After doing the cost-benefit analysis of the different potential solutions to designing the SAUSER system it was decided to implement the quadcopter design. The quadcopter design is fairly simple but the implementation of the various subsystems and their integrations with each other requires careful consideration and design approach. Subsystems such as GPS module for navigating through the space, ultrasonic sensor for obstacle avoidance and PIR sensor for motion detection act as nodes of the overall system. Other factors like weight, thrust, power requirement and range were also analyzed to achieve the required design goals.

FEA and CFD analysis of the CAD design was done using the SolidWorks to analyze the fluid interactions with the surface of the drone when in flight so as to verify the performance of the drone to perform mission under potential flight environment scenarios.

The team also be utilized physics-based modeling to verify the results of the computer-aided engineering analysis. The physics-based model utilized the analysis techniques taught in the SAUSER team's Mechanical and Aerospace Engineering coursework at Kennesaw State University. The material that was utilized came from the following courses:

- Aerodynamics (ISYE 3801)
- Aircraft Design and Performance (ISYE 3801)
- Circuits Analysis I (EE 2301)
- Helicopter Theory (ISYE 4802)
- Strengths of Materials (ENGR 3131)
- Machine Design (ME 4141)

3.2: Design Requirements and Specification

After careful consideration of the distinct designs for the drone, multi-rotor quadcopter design was selected as multi-rotor drones provide greater control and maneuverability. They have ability to hover, can take off and land vertically compared to fixed wing and single rotor design. The design requirements and specification for the

SAUSER were formulated such that design goals can be achieved and SAUSER will be able to complete its mission successfully. The proposed requirements and specifications for the SAUSER system are as follow:

- Quadcopter design
- Max take-off weight of 13 lbf.
- Payload capacity of 2lbf
- Max Service Ceiling 5000m @MSL
- Wireless charging system
- Max speed of 22 m/s or 50 mph
- Maximum Flight time of 45 minutes
- Thrust to weight ratio of 3.0.
- Vertical takeoff and landing (VTOL) capability
- Hovering capability
- Satellite positing system
- Obstacle Sensing system
- Live Video and audio data streaming capability
- Remote control and semi-autonomous piloting system
- Initial design dimensions: Length 17 in, Height 10 in and Width 17 in.

3.3: Minimum Success Criteria

The minimum success criteria for the SAUSER system were determined based on the design goal and requirements and it should achieve the following:

- Meet defined design requirements and specifications
- Complete project SAUSER by the end of semester
- Accomplish the design within the bounds of budget
- Develop Optimized design from the trade studies.
- CAD (Computer Aided Design) of the prototype
- CFD and FEA analysis to test and prove minimum performance requirements

3.4: Mission Profile

The mission profile shown in Figure 2 depicts the various stages of the flight that SAUSER drone will go through as it performs its typical mission. The drone takes off vertically from its docking station and climbs to the cruising altitude of 1000 ft when in flight to the target location.

When close to the target location drone descends to desired altitude to perform it mission of surveillance and emergency response depending on the circumstances for approximately 30 minutes. In the next stage it climbs back to the cruise altitude and when close to docking station it descends and lands vertically at the station where recharges for future missions.

The overall flight time of the drone was planned to be 50 minutes by the power available from onboard batteries. It is able to perform all mission within this time while meeting the criteria listed under minimum success criteria. In the first half of the mission the flight time to target at the max distance (8 miles radius from the docking station) is expected to be 10 to 11 minutes. In the return flight to the dock, it would take 8 to 9 minutes which is lesser than the time it took to reach target because in return flight it would not need to recalculate and adjust its flight path completely as it can follow the same navigation instruction just in reverse order which would shave off 2 or 3 minutes from its return flight time.

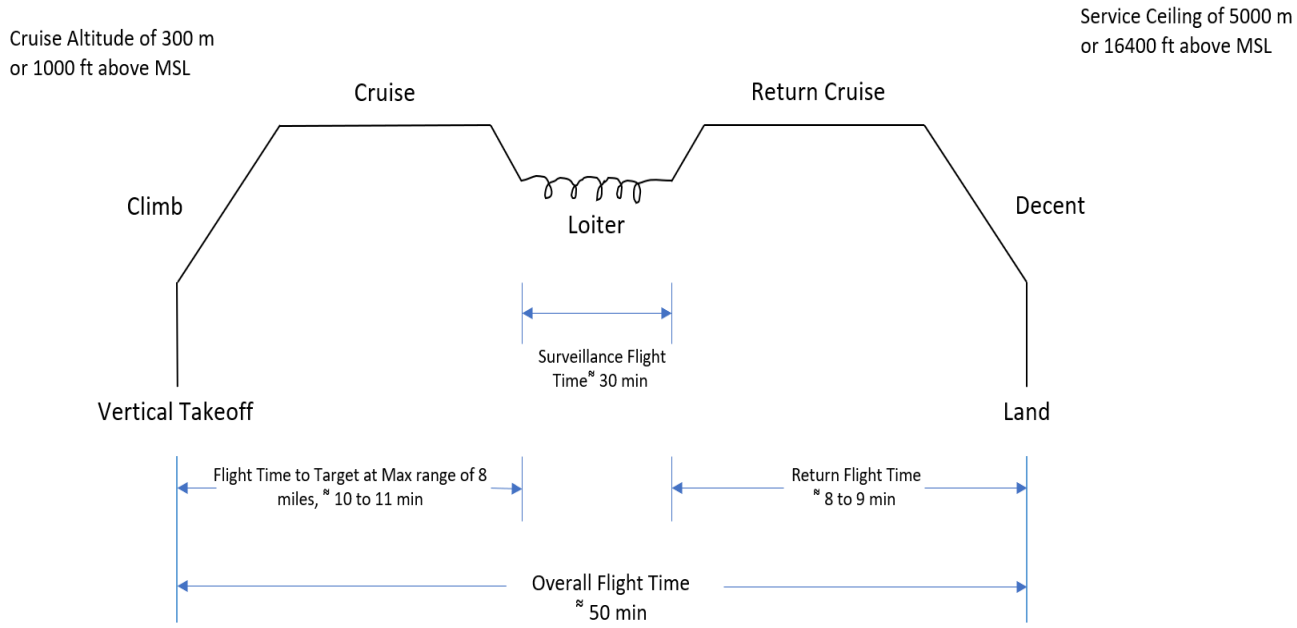

Figure 2: Mission profile

3.5: Conceptual Design Sketches

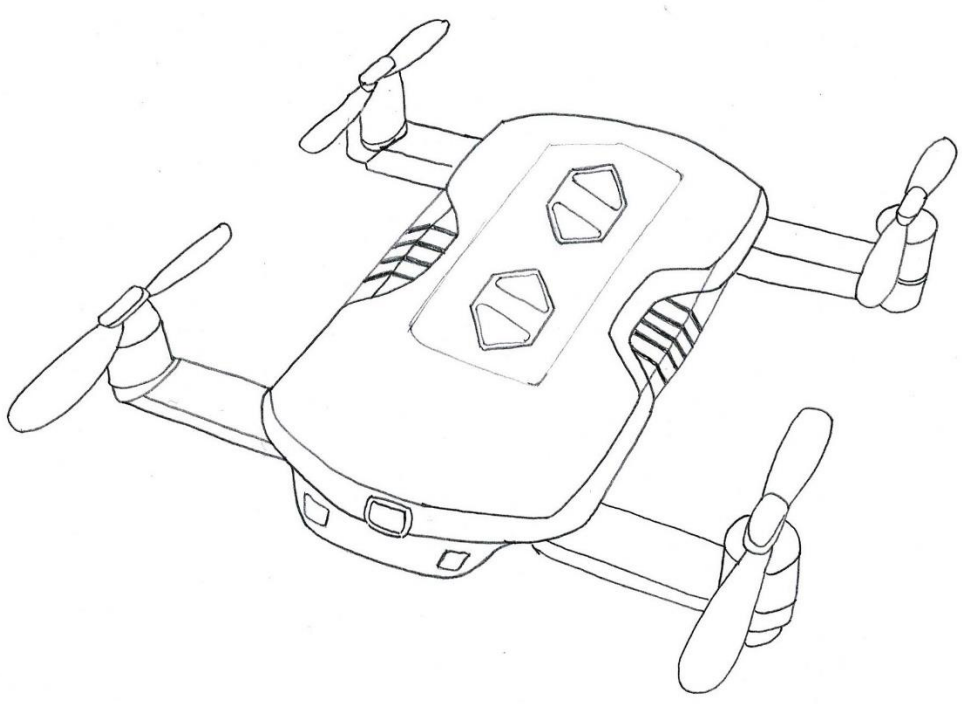

Figure 3: Initial conceptual design sketch 1 of the SAUSER.

Figure 3 is the first sketch of the potential design with basic drone geometry.

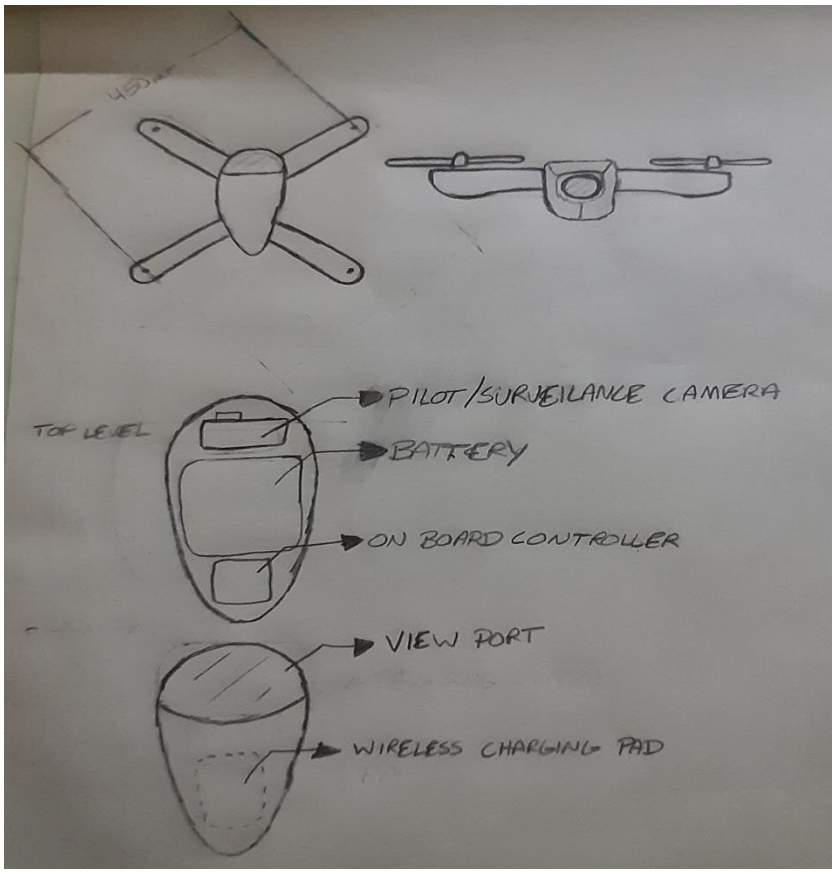

Figure 4: Initial conceptual design sketch 2 of the SAUSER.

Figure 4 is a second concept sketch that includes some more details such as spaces for various electronic components.

3.6: Trade Study Items

Items that will be analyzed in the trade study will be weight, range, speed, and endurance. Range and endurance need to be maximized with the consideration of weight to allow for the completion of missions.

The weight of the drone effects the flying capabilities of the drone by increasing or decreasing the disk loading on the propellors. The weight will be reduced by using lighter, stronger, materials for the chassis and energy dense cells in the battery.

The range is the distance the drone will be flying from the dock. To cover more rural areas, the drone will have to be able to fly a long distance and return to the dock on one charge.

Battery capacity refers to the power that can be drawn from the battery. Increasing the cells in the battery will increase the capacity but will make the drone weight more. Having energy dense cells will help to increase the capacity with lighter battery cells. The volume of the battery will also have to be considered to maintain a low-profile drone body.

Responding to emergency situations as fast as possible is a priority for the drone. The speed of the drone will be optimized for the average flight scenario, but I can also be changed by the drone pilot during the flight depending on the flight conditions. Weight and battery capacity will also be considered for the speed trade study.

The endurance for the drone is how long it can hover at the scene. The endurance and range of the drone will have to be balanced to balance enough of each aspect. The drone will be dispatched to the scene for its entirety to capture footage. This item is also dependent on the battery capacity of the drone.

3.7: Budget

The cost per drone and dock was expected to stay under $2000. The bulk of the budget was directed to connecting to the infrastructure to support the Wireless Local Area Network for the drone docks. An existing drone flight software for controlling the drones was used and integrated with the system. Each package can be tailored to the city it will be operated in and infrastructure system work will be done at the 911 call centers to cater the drone system. For a package of 40 drones and docks with installation, a server for video, training on drone piloting, and other services for operation, the expected budget will be $4,000,000 for a ten-year period.

3.8: Materials Required

Different components of the drone experience different amounts of stress when in flight or in unavoidable crash thus requiring the use of different materials to make them. The proposed materials for the components and the reason for their selection is explained below in detail.

Rotors: The rotor is one such component that experiences majority of the forces when in flight and is also most likely to get damaged in crash therefore it needs to be made of a stronger material while also being light in weight to reduce power consumption. Rotors made of Carbon fiber or other reinforced composites are being used as they can provide the required structural strength while weighting significantly less if they were to be made of metal such as aluminum.

Underbelly charging unit: A section of the underbelly has ceramic or tempered glass surface in order to facilitate the wireless charging of the drone through induction coils. Plastic or metal surface interfere and reduce the efficiency of the charging through induction coils which is why ceramic or tempered glass is the preferred choice.

Fuselage: The fuselage or main body of the drone needs fair amount of structural integrity so as not to fracture at least in case of hard landing or a crash from a low altitude. It would be expensive and out of the budget constraints to have drone body made of carbon fiber even though it provides required structural integrity therefore 7075-T6 aluminum was used which has the added benefit of being cheaper and stronger even though it would weigh more if the body was made of carbon fiber or other composites.

Table 1 shows a table depicting the potential material that will be selected for different components after evaluating the said materials based on selection criteria. The mechanical properties of these materials will be analyzed to make certain that the finalized material for each component will perform successfully under the expected environmental conditions during the flight.

Table 1: The potential material for components and their selection criteria.

Components	Material	Selection Criteria
Rotor	Carbon Fiber-reinforced composites (CRFCs)	Structural Strength, Light Weight
Underbelly Charging Unit	Tempered Glass or ceramic	Should facilitate efficient Induction charging.
Fuselage	Aluminum alloy 7075-T6 or Thermoplastics such as Polystyrene, Nylon	Cheaper, Lighter and Stronger

3.9: Resources

The available resources are sorted into three categories: people, literature, and software.

3.9.1: People

- Dr. Adeel Khalid (course instructor and faculty advisor for the aerial robotics team)

3.9.2: Literature

- Literature for UAV's that can perform missions similar to that of our project.
- Kennesaw State University Sturgis Library and Johnson Library (including inter-library loans)
- Kennesaw State University academic journal subscriptions
- Textbooks for relevant engineering coursework (Aerodynamics, Helicopter Theory, Strength of Materials, etc.)

3.9.3: Software

- SOLIDWORKS (including Flowsim and Simulation computer-aided engineering packages)

- AutoCAD
- MATLAB

3.10: Team Assignments/Schedule

See attached Gantt chart for scheduling and team assignments. Ryan Foster acted as project manager for this project.

Semi-Autonomous UAV design for Surveillance and Emergency Response

Kennesaw State University
Ryan Foster, Kenneth Jones,
Arshdeep Sandhu

Project Start: Mon, 1/11/2021
Display Week: 1

TASK	ASSIGNED TO		START	END
Concept Design				
Design requirements	Arshdeep	100%	1/11/21	2/15/21
Rotor configuration	Ryan	100%	2/15/21	3/8/21
Structure configuration	Kenneth	100%	2/15/21	3/8/21
Control/power configuration	Kenneth	100%	2/15/21	3/8/21
Sizing calculations	Arshdeep	100%	2/15/21	3/8/21
Component Design/Selection				
Rotor design/selection	Kenneth	100%	3/8/21	3/29/21
Structure design/selection	Kenneth	100%	3/8/21	3/29/21
Control/power selection	Arshdeep	100%	3/8/21	3/29/21
Verification/Analysis				
CFD Analysis	Ryan	100%	3/29/21	4/19/21
FEA stress analysis	Ryan	100%	3/29/21	4/19/21
CFD/FEA results verification	Ryan	100%	3/30/21	4/12/21
Final performance analysis	Everyone	100%	3/29/21	4/19/21
Miscellaneous				
Bill of materials	Kenneth	100%	3/29/21	4/19/21
Economic Analysis	Ryan	100%	4/14/21	4/20/21
Poster	Arshdeep	100%	4/14/21	4/28/21
Video	Kenneth	100%	4/14/21	4/28/21
Presentation	Everyone	100%	4/14/21	4/28/21
Report writing	Everyone	100%	1/11/21	4/28/21

Figure 5: Project task assignment and their proposed completion schedule.

An expanded version of this Gantt chart containing a visualization of the dates and progress, can be found in Appendix D: Gantt Chart.

Chapter 4: Concept Alternatives

4.1: Helicopter Alternative

Single rotor, helicopter, drone designs have the opportunity for more efficient systems. Helicopters use lower speeds and lager blades on a main rotor to allow for more efficient hovering. Although the higher efficiencies, the single rotor was not chosen for this design.

Helicopters have a large main rotor and a small tail rotor. The incorporation of the tail adds a level of complexity in design. Mounted on a plane perpendicular to the main rotor plane, the tail rotor counteracts the moment created by the main rotor. It can either push or pull the aircraft in the right heading. The geometry of the tail would then have to be optimized for distance from the main rotor.

Quadcopters are simpler in that the four rotors spin in 2 directions to counteract each other. The structure of the quadcopter can be a square and the craft will be naturally more balanced. Using sensors on the drone, stability can be maintained by throttling the motors individually.

The single rotor design lends to instability, especially in nonstandard day weather. The vibrations caused from the large main rotor would not aid well in surveillance. Even on a gimbal, the constant vibrations from the large rotor would risk ruining the footage of emergency events. The quadcopter design is an industry standard for taking drone footage. The drone is more balanced and has the ability to adjust during hover leading to clear footage.

Single rotor drones also pose a possible threat to personal safety and property. The blades for single rotor drones have to be longer and sharper compared to quadcopter blades. The size paired with higher torque can lead to worse injuries if it were to hit a person. Scratches and lacerations have been recorded due to quadcopters, but RC helicopters and single rotor drones have caused severe injury and fatalities, although extremely rare. A possible death from a public safety drone does not bode well for the system. Quadcopters are less likely to damage someone from the rotors, so they would be a safer option for this design.

4.2: Landing Gear Alternatives

One concept for optimizing this design for a traffic response application is in the landing gear. Many drones feature long landing gear allowing the drone to land in a variety of environments and situations. Figure 6 illustrates this idea:

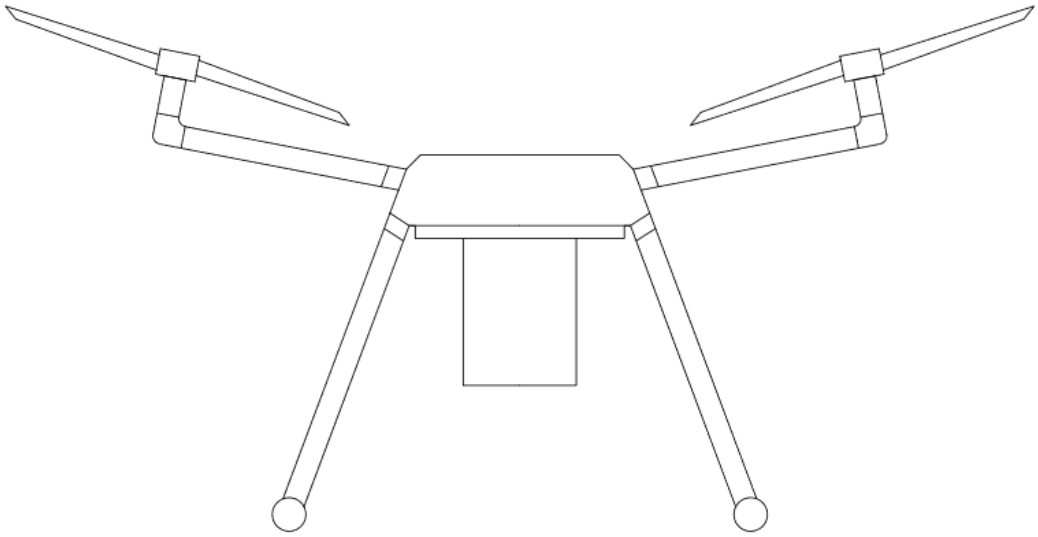

Figure 6: Concept sketch of long landing gear alternative.

However, for our application of short flights to quickly gather preliminary information and allow dispatchers to send in first responders, landing gear may not be necessary. Figure 7 illustrates this idea:

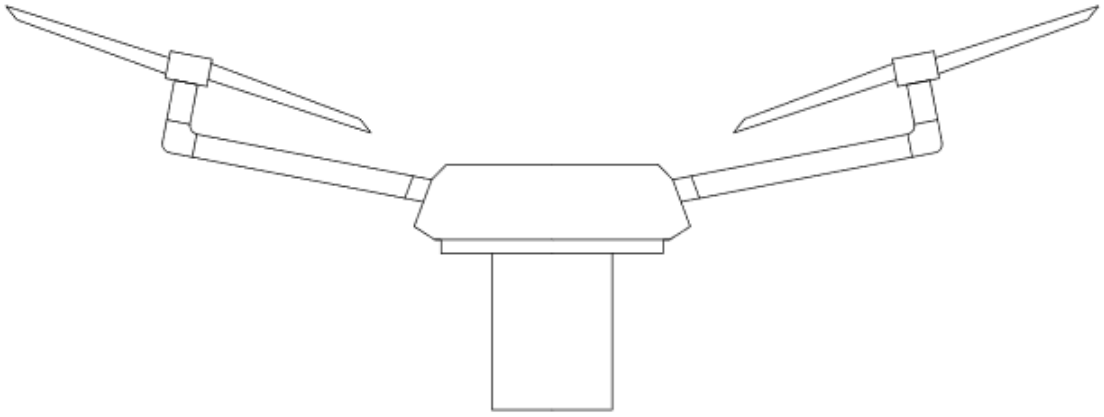

Figure 7: Concept sketch of no landing gear alternative.

One additional concept is a mixture of the previous two alternatives. The drone could have short landing gear allowing it to land only on flat pavement. Since roads are generally very flat (especially at traffic lights), landing gear may be very short to simply allow the drone to land which waiting for first responders to arrive. Because this drone will only be landing on controller, previously engineered, surfaces, this may be sufficient. Figure 8 illustrates this idea:

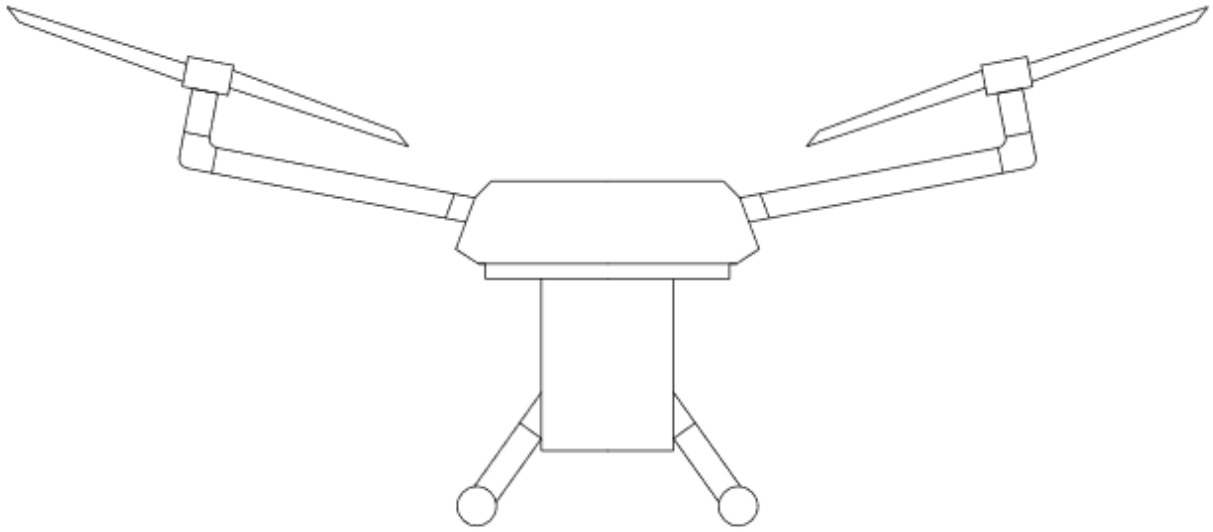

Figure 8: Concept sketch of short landing gear alternative.

The Kennesaw State University engineering team has decided to use the no landing gear alternative. This selection was made because the addition of short landing gear would interfere with the wireless charging system. The long landing gear alternative would increase the weight of the drone and leave less weight for batteries. The increase in flight time was prioritized over the added ability to land.

Chapter 5: Electronics

5.1: Sensors

5.1.1: Accelerometers

Drone orientation is key in flying the drone remotely. Accelerometers detect the movement of the craft and can relay the position of the craft to the pilot. Accelerometers can also be used to monitor motor vibrations.

5.1.2: Tilt Sensors

Tilt sensors are another sensor that determines the orientation of the craft. Tilt sensors help to maintain stable flight alongside the gyroscopes and accelerometers.

5.1.3: Current Sensors

Current sensors measure the current draw of the motors. Power consumption is important for battery life, flight time, and system protection. These sensors can provide information on faulty motors during system diagnostics. A current sensor will be used onboard the power distribution board to measure current draw.

5.1.4: Inertial Measurement Unit

These measure the speed, direction, and orientation of the craft. The IMU provides data to the FC for autonomous landing sequences.

The IMU for the prototyping phase of the SAUSER is a Pixhawk4. This device utilizes the aforementioned sensors to give stability data. The Pixhawk also allows for control over the motor speed through the Electronic Speed Controller. The Pixhawk is connected to the WiFi Access point to allow for control over WiFi. The Pixhawk controller can be seen below in Figure 9.

Figure 9: Pixhawk - Inertial Measurement Unit.[19]

5.1.5: Camera

The camera is the most important part for the user. The camera records the incidents for possible inspection after the event. Video is transmitted from the camera to a repository server.

The selected camera is a GoPro Hero 9. This is a camera well known in drone videography for its ultra-high-definition video and rugged design. The camera is housed inside the drone to prevent water intrusion and is mounted on a gimbal for stability. A video transmitter was referenced in the block diagram, the Hero 9, when connected to internet, uploads video to the cloud through a GoPro account. Using the WiFi access point on the drone, the video automatically uploads video without user input. The Hero 9 also has a microSD card for hard storage. A display photo of the GoPro Hero 9 can be seen below in Figure 10.

[19] *PIXHAWK Fligt Controller for Helicopter, Racing Drone, Fixed Wing, Airplane, Glider, Cars and Boats*, RadioLink, www.radiolink.com/pixhawk.

Figure 10: Camera - GoPro Hero 9[20]

5.1.5: Gimbal

Gimbals provide stability and dampening for cameras and other gear. Motorized gimbals use Pan, Tilt, and Poll to stabilize the camera by counter acting the pitch, roll, and yaw of the drone body. Although the drone may be stable, the dampening provided by the gimbal alleviates any vibrations caused by the rotors. The gimbal also gives the user the ability to focus the camera on the incident.

The Gimbal chosen for the prototype model is a Feiyu Tech G3 Gimbal. This gimbal has 2 rotational axis of rotation. The gimbal mount has rubber dampening boots to limit vibration. This gimbal is made to fit GoPro action cameras, but there are modifications to camera arm to allow for a charging cable. The Pixhawk pinouts will be used to control the motors and a cable from the PDB will power the gimbal. The brushless motors run on 7-17 volts, so the chosen

[20] "HERO9 Black." *GoPro*, GoPro, gopro.com/en/us/shop/cameras/hero9-black/CHDHX-901-master.html.

battery will be sufficient. The chosen gimbal holding a GoPro Hero 3 can be seen below in Figure 11.

Figure 11: Feiyu Tech G3 Gimbal[21]

5.2: Power Electronics

5.2.1: Electronic Speed Controller (ESC)

ESC's are responsible for throttling the motors as well as converting DC power from the batteries into 3 phase. The ESC is a circuit that takes input from the flight controller to change the speed of the motor. A 3 phase sinusoidal wave is produced to provide smooth and efficient power. The ESCs for this project are built into the Power Distribution Board. The Pixhawk uses signal wires to throttle the motors through the common board.

5.2.2: Flight Controller (FC)

The main function of the flight controller is to receive the input for the command center and execute the commands. All the sensors on the drone provide information to the FC. The FC

[21] "FeiyuTech G3 3-Axis Brushless Gimbal for Multi-Rotor or Aircraft." *Hobbyking*, Hobbyking, hobbyking.com/en_us/feiyutech-g3-3-axis-brushless-gimbal-for-multi-rotor-or-aircraft.html.

sends the data back to the command center for user interpretation and can also use the data to make autonomous adjustments. Gyroscopic data can be used to maintain stable flight autonomously. A landing program can also be executed autonomously using distance data. The ESC signal cables are connected to the board so that the motor speeds are driven by the FC.

The Pixhawk acts as the flight controller for the prototyping stage. It houses the needed sensors and executes commands through the same device. The Pixhawk has an array of signal pins to control the motor speed, gimbal motors, and other auxiliary electronics.

5.2.3: Power Distribution Board (PDB)

Power from the battery is sent to the PDB for distribution to other parts of the drone. A majority of the power will go to the ECS's. The PDB has shunts to protect from current spikes and also house the current sensors. A discrete PDB was chosen as opposed to a flight controller with power distribution for added safety for the electrical components.

The iFlight SucceX-E was chosen for the PDB. This features integrated ESC's and onboard current sensors. This device is rated for a 5S Lithium Polymer Battery; this means the PDB can withstand a maximum of around 21 volts. The maximum current for the board is 45 Amps. Further literature review will be done to investigate if either onboard of discrete ESC's would be ideal for the SAUSER. The PDB is depicted below in Figure 12.

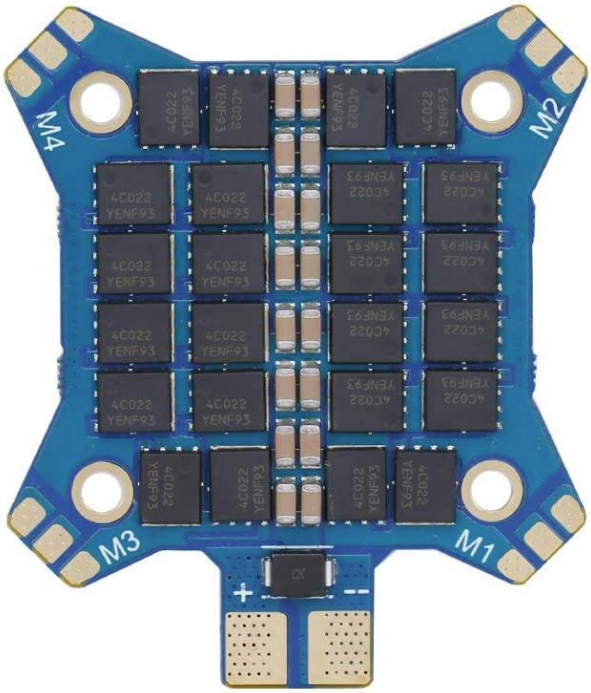

Figure 12: Power Distribution Board - iFlight SucceX-E[22]

5.2.4: Brushless Motors

The drone motors are 3 phase DC brushless motors. Brushless motors use permanent magnets around a 3-phase coil to induce high rotational speeds. The bell of the brushless motor has a threaded post for the propellor to tighten on to. The motors can go both clockwise and counterclockwise. The direction will be set by the FC and corresponding propellers will be fitted.

The chosen power train for the prototype SAUSER is the iFlight 2208 2450KV motor. The KV factor for the motor is the revolutions per minute of the rotor per volt. These motors support a 4S battery that has a 14.8 volt to 16-volt maximum potential. These motors use the 16 mm standard for mounting holes for easy replacement. Figure 13 shows 4 of the brushless motors mentioned.

[22] "SucceX-E 45A V2 2-6S BLHeli_S 4-in-1 ESC." *IFlight*, IFlight, shop.iflight-rc.com/index.php?route=product%2Fproduct&path=20_27_136&product_id=1413.

Figure 13: Brushless Motors - iFlight 2208 2450KV[23]

5.2.5: Battery

The drone battery is made of 3.7-volt lithium-ion cells. These cells are added in series to have an appropriate voltage potential and added in parallel to increase the storage capacity. The battery has an MX60 connector to the power distribution board and a multi wire connector for the BMS. The battery has layers of insulation to keep the cells protected from impact. This battery will be an off the shelf component used for hobby and drone purposes.

[23] "XING-E 2208 2-6S FPV Motor." *IFlight*, IFlight, shop.iflight-rc.com/index.php?route=product%2Fproduct&path=20_26&product_id=881.

The current battery selected is the Turnigy 14.8-volt, 5.0-amp hour, lithium battery. This battery weighs 586 grams for 74-Watt hours of power. Each drone may need more capacity than 1 battery provides, so more batteries may be needed, or larger batteries may be used. This line of batteries was chosen because Turnigy is a respected brand in the hobby and drone industry. Batteries in this specific line are hard cased in plastic to protect from impact. The chassis of the drone will protect the battery, but the added protection is necessary. Lithium batteries are prone to ignition and possible explosion if punctured. The Turnigy battery selected is shown below in Figure 14.

Figure 14: Turnigy 14.8-volt 5.0-amp hour Battery[24]

[24] "Turnigy 5000mAh 4S1P 14.8V 20C Hardcase Pack." *Hobbyking*, Hobbyking, hobbyking.com/en_us/turnigy-5000mah-4s1p-14-8v-20c-hardcase-pack-1.html.

5.2.6: Battery Management System (BMS)

The BMS is the charging unit for the battery. Each cell is charged individually at a balanced rate. The BMS provides under-voltage protection to the battery and regulates the current flow into the battery.

Coordination will have to be made with the company, Wibotic, for their aerial robotics solutions. Wibotic has a battery charger that is intended to work with their charging system. This battery charger will operate as the BMS for the LiPo battery. The battery charger will regulate the power into the battery to provide for safe charging and prevent the battery from overcharging. Overcharging can lead to heat, decreased battery life, and possible battery bloating. Battery bloating is dangerous, as the battery could rupture and cause a fire. The Wibotic production photo for the OC-110 is provided in Figure 15.

Figure 15: OC-110 Onboard Charger[25]

[25] "Products." *WiBotic*, 27 Apr. 2021, www.wibotic.com/products/.

5.2.7: Wireless Charging Coil

The wireless charging coil and the wireless charging pad uses an electromagnetic field to induce a current in the coil. This allows for the drone battery to stay inside the drone and negate the use of a port for charging.

Wibotic also provides a solution for wireless drone charging. The first component in the system is the receiver coil. This will be mounted on the bottom of the drone for charging at the dock. The second component is the transmitter coil. This is a similar coil that is mounted in the dock, so the drone lands directly on top of the transmitter coil. The final part of the system is the transmitter. This is basically a power supply that converts the 120-volt 60 hz AC power from the street into 15-volt high frequency wireless DC power.

Wibotic also provides a solution that has a transmitter and transmitter coil in one landing pad. This will be investigated for possible applications as well. The Wibotic production photo for the RC-100 is provided in Figure 16.

Figure 16: RC-100 Receiver Coil[25]

5.2.8: Telemetry Radio

The telemetry radio is the onboard avionics of the drone. The telemetry radio sends the data from the flight controller to the command center and the command center sends commands to the telemetry radio for the flight controller.

For the prototyping stage of the SAUSER, an Nvidia Jetson Nano was used for the telemetry radio. This is a Wi-Fi access point on the drone. This was only used in prototyping to test Arducopter autonomous commands and work in place until a more streamlined and simpler device is developed. The Wi-Fi Access point provides access to command the flight controller over the internet. The Pixhawk connects to the Jetson using a USB type B to A cable. ArduPilot was used to allow for the Robot Operating System (ROS) commands to be executed. Literature is currently being reviewed from IEEE conferences on this topic. The Nvidia Jetson Nano is shown in Figure 17.

Figure 17: Nvidia Jetson Nano[26]

[26]"Jetson Nano Developer Kit." *NVIDIA Developer*, Nvidia, 14 Apr. 2021, developer.nvidia.com/embedded/jetson-nano-developer-kit.

5.3: Charging Dock

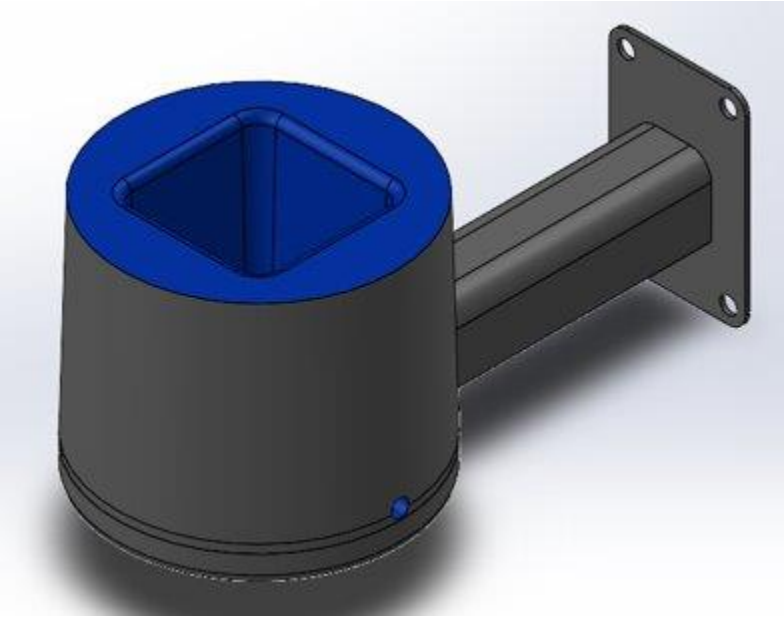

Figure 18: Docking station CAD model

The CAD model for the dock is shown above in Figure 18. The Charging dock has an aluminum outer construction for strength and durability. The cup shaped inner portion of the dock is made of plastic to ensure proper charging. This design will be mounted to the top of a traffic pole using bolts and a service station will be located lower on the pole towards the ground.

5.3.1: Transmitter Coil

The Transmitter coil is a copper coil that emits high frequency electromagnetic waves to transmit power. To optimize the power transmission, a non-metal surface should be between the transmitter and receiver coil. These components will also need to be safe from the elements; the transmitter coil will be housed under the landing surface of the dock. The Wibotic production photo for the TC-200 is provided in Figure 19.

Figure 19: TC-200 Transmitter Coil[25]

5.3.2: Transmitter Power Supply

The power supply takes the 120-volt AC current from the city power grid and converts it into a high frequency signal. The coil and power supply are connected by a coaxial cable. This component will be held in a serviceable box near the ground at the docking site. The TR-110 supports up to 125 W for charging. This component is also able to monitor and controller over the internet using a Wibotic application, so it will be connected via ethernet to the Wireless access point at the docking station. The Wibotic production photo for the TR-110 is provided in Figure 20.

Figure 20: TR-110 Transmitter Power Supply[25]

5.3.3: Wireless Access Point

Pilots are miles away from the drone, so the only way to be able to connect to the drone is over the internet. The WiFi Access Point on the drone will connect to a ground unit at a dock. A Wireless Access Point (WAP) will be installed at the docking unit and all the WAPs will form a grid, much like the cell tower grid cellphones use. This network will be private and for this drone system and possibly other communications networks for public services.

Chapter 6: Sizing

The detailed analysis of the overall design of the SAUSER is affected significantly by the mass and therefore weight of the drone. The sizing was done in order to account for the mass and weight of each module, components that were used in the SAUSER. The mass of the components that were designed in SOLIDWORKS was determined using mass properties tool in SOLIDWORKS and the mass of the off-shelf components were obtained from the specification data provided by the seller or manufacturer.

Table 2: Power module mass and weight

Power Module	**Mass (kg)**	**Weight (N)**	**Weight (lbf)**
Battery (4 pack)	1.271	12.473	2.804
Battery charger	0.162	1.59	0.357
Wireless charger	0.069	0.68	0.153

Table 2 shows the mass and the weight of the components that constitute the power module which provide the power to motors and other sensors of the drone. It contains the charging unit for the battery along with wireless charging through induction plate. The mass of these components was obtained from the seller as the components were not designed and manufactured in house to reduce the complexity of design process.

Table 3: Sensor module mass and weight

Sensor Module	Mass (kg)	Weight (N)	Weight (lbf)
PDB & ESC	0.0144	0.14	0.0315
FMU	0.0363	0.36	0.0809

Table 3 lists the mass and weight of the Sensor module which consist of the electronic speed controller, power distribution board and the FMU. These were selected based on the design goal requirement and its use is explained in detail in the electronic section of the report. Since these are commercial off-the-shelf components so their mass was obtained from specifications listed by the seller.

Table 4: Camera module mass and weight

Camera Module	Mass (kg)	Weight (N)	Weight (lbf)
Gimbal	0.178	1.75	0.393
Camera transmitter	0.159	1.56	0.351

Table 4 shows the mass and weight of the components which constitute the Camera module of the drone. Gimbal contains the camera and motorized joints for freedom of motion of the camera to provide 270 degrees of view. Camera transmitter unit sends the live audio and video from the drone to the control center for monitoring and recording. Since the components for camera module were off-shelf commercial parts therefore their mass and weight were also obtained from the specifications listed by the seller.

Table 5: Fuselage components mass and weight

Fuselage Component	Mass (kg)	Weight (N)	Weight (lbf)
Fuselage	1.292	12.677	2.85
Arms (x2)	0.997	9.786	2.2
Motors	0.250	2.45	0.551
Rotor Blade (x4)	0.062	0.609	0.137
Miscellaneous	0.544	5.337	1.2

Table 5 refers to the mass and weight of the components that constitute the Fuselage and other major components of the drone body. The mass of the fuselage, arms and rotor blades were determined using the mass properties tools in SOLIDWORKS as these major components were designed from ground up based on the design goal of the SAUSER. The mass of the motors that propel the four rotor blades was obtained from the manufacturer provided specifications. The miscellaneous mass and weight are listed to account for the mass of the parts such as screws, rivets, wires etc. that are used in joining the drone body parts and linking the other modules together to work as a complete unit.

Table 6: Design max take-off weight of the SAUSER

Design Weight	N	lbf
Payload capacity	8.896	2
Max take-off weight	57.826	13.108

To conclude, Table 6 list the payload capacity and the max take-off weight of the SAUSER. It was obtained by accounting for the mass & weight of the various components listed

in the other tables as discussed earlier in this section. The max take-off weight was determined to be 13.108 lbf which is sufficiently close to our initial design goal of 13 lbf.

Chapter 7: Rotor Design

The rotor blades are one of the most important components of the SAUSER as they provide the required lift for all possible flight conditions as described in the design approach section of the report. The rotor blades are made of Hexcel AS4C 3k carbon fiber which has a tensile strength of 685000 psi making it 9 times stronger than the AISI 304 steel thus giving it required strength to operate under various forces acting on it while in hover, forward flight or any other flight scenario. Hexcel carbon fiber provides an added benefit of being lighter in weight which is helpful in reducing the overall weight of the drone thus requiring less thrust and power consumption to fly.

Figure 21 shows the top view of the Rotor which was designed using SOLIDWORKS. The rotor consists of two blades which are joined at the central hub with radius of the Rotor being 167.01 mm and the diameter of the hub measuring to be 9 mm.

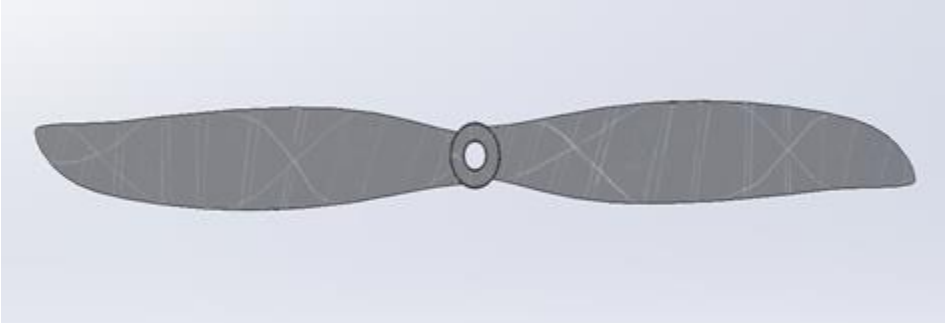

Figure 21: Top view of the rotor modeled in SOLIDWORKS[27]

Rotor blades has a twist of 7.25 degrees to obtain approximately uniform amount of lift along the profile of the blade. Figure 22 shows the twist in the airfoil of the blade as it can been seen from the side view.

[27] P. S. (2021, February 26th). Aeronaut CAM Carbon Light 13x5 Propellor. **https://grabcad.com/library/aeronaut-cam-carbon-light-13x5-propeller-1**

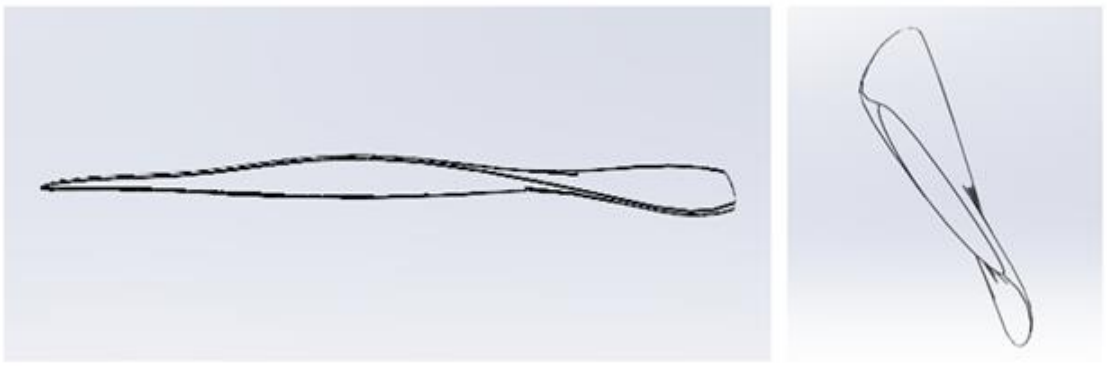

Figure 22: Side view of the rotor blade showing the twist in its airfoil

SAUSER being a quadcopter has four rotors in total and the two rotors on the right rotate counter-directionally to the rotors on the left thus acting as a counter torque mechanism. The detailed CFD analysis was done to analyze the thrust output of the rotor spinning at different rpms, thrust to weight ratio and % power consumption which is explained in detail in the CFD analysis section of the report.

The BEMT theory was used to calculate the coefficient of thrust, thrust produced by the single rotor, induced power coefficient, induced power, profile power and total power consumed by the drone when in hover.

Chapter 8: Detailed Analysis of SAUSER (In Hover) Using BEMT

The Blade Elemental Momentum Theory was used to calculate various parametric values when the SAUSER is in the hover flight and the calculations shown in Table 7 are for the single rotor. The detailed calculations are shown in the Appendix C of the report.

8.1: Assumptions

Before getting into the specifics of the analysis, there are a few conditions that must be assumed. These assumptions allow for an ideal comprehensive analysis to take place. Necessary assumptions include:

- The SAUSER is in hover
- Operating in standard day conditions at sea level

8.2: Rotor Design Power for Single Rotor

The single rotor specifications are calculated while in a hovering state. The climb velocity (λ_c) will be assumed to be 0 since the drone is not climbing.

The rotor induced inflow ratio (λ_i) is the ratio of the velocity parameter to the velocity at the tip and it can be calculated using the following equations.

$$V_{tip} = 2\Omega\pi R \text{ m/s}$$

$$\lambda_i = V_{tip}/(\Omega R)$$

The coefficient of thrust (C_T) is a nondimensionalized relation of the dynamic pressure and area of the disk. C_T was calculated using the second equation shown below.

$$C_T = \frac{T}{\frac{1}{2}\rho(R\Omega)^2 \cdot A}$$

Or

$$C_T = 4 * \int_0^1 (\lambda_c + \lambda_i) * \lambda_i * r dr$$

The thrust of the single rotor (T) is the force produced by the propeller of the drone upwards. Since we are calculating the thrust of a single rotor therefore it only needs to support enough thrust to just support ¼ the total weight of the drone (quadcopter).

$$T_{MR} = C_T * \rho * A * (\Omega R)^2$$

The induced power factor (*k*) is a correction factor based on the load factor (n).

$$k = \frac{2(n+1)^{\frac{3}{2}}}{(3n+2)}$$

The induced power coefficient (C_{pi}) is a nondimensionalized form of the induced power. The induced power (P_i) is the power required to hover.

$$C_{pi} = (\sqrt{2})^{-1} * k * C_T^{\frac{3}{2}}$$

$$P_i = C_{pi} * \rho * A * (\Omega R)^3$$

The Profile Power (P_0) is the power needed to overcome viscous forces on the rotor. The rotor must overcome the drag on the blades to spin, adding to the required power. The coefficient of Profile Power (C_{P0}) is the nondimensionalized form of P_0. The coefficient of drag at zero lift (C_{d0}) is the coefficient version of the drag the rotor encounters when no lift is being generated; the C_{d0} was approximated using a chart to be .011.

$$C_{p0} = \frac{\sigma}{8}\left(C_{d0}\right)$$

$$P_0 = C_{p0} * \rho * A * (\Omega R)^3$$

The Total power (P_T) is the summation of the powers used to fly according to the set parameters. This considers the profile and induced powers. The coefficient of total power (C_{PT}) is the coefficient form of the total power.

$$C_{pT} = C_{pi} + C_{p0}$$

Table 7: Calculated values for power for the single rotor when in hover

BEMT With sectional C_d, C_T and some losses		
λ_C	0.00000	
λ_i	0.373	
$C_T = 4 * \int_0^1 (\lambda_c + \lambda_i) * \lambda_i * r dr$	0.278	
$T = C_T * \rho * A * (\Omega R)^2$	14.441	N
$k = \frac{2(n+1)^{\frac{3}{2}}}{(3n+2)}$	1.131	
$C_{pi} = \left(\sqrt{2}\right)^{-1} * k * C_T^{\frac{3}{2}}$	0.117	
$P_i = C_{pi} * \rho * A * (\Omega R)^3$	133.711	W
$C_{p0} = \frac{\sigma}{8}(C_{d0})$	0.000077	
$P_0 = C_{p0} * \rho * A * (\Omega R)^3$	0.0879	W
$C_{pT} = C_{pi} + C_{p0}$	0.11707	
$P_T = C_{pT} * \rho * A * (\Omega R)^3$	133.79	W

The total thrust produced by the drone when in hover will be the sum of the thrust produced by its 4 rotors i.e.

Total Thrust = 14.441 N * 4

Total Thrust = 57.764 N

The Thrust to weight ratio of a similar drone in market was approximately to what we got for SAUSER which gave the assure that our calculations using the BEMT were valid and correct.

Chapter 9: Simulations

9.1: Computational Fluid Dynamics (CFD) Analysis

9.1.1: CFD for Rotor Blades

CFD analysis of the rotor blades was done using SOLIDWORKS Flowsim. A trade study of the blades at different RPM was done to determine the thrust provided by the blades. The motors selected for this study can provide 2250 RPM/Volts and will be supplied with 14.8 Volts. This means that the motor can provide 33,300 RPM. Specifics of the SOLIDWORKS settings can be found in Appendix A. Figure 23 shows the flow trajectories of this rotor blade analysis.

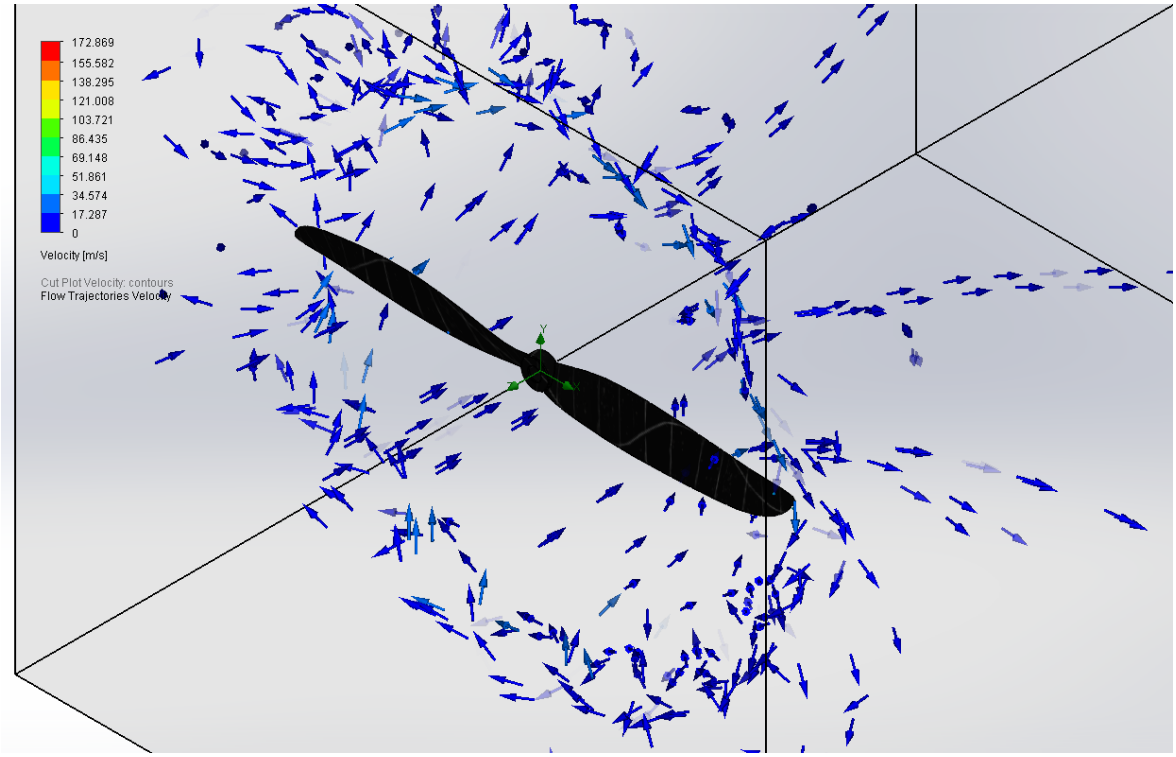

Figure 23: The flow trajectories of the rotor analysis

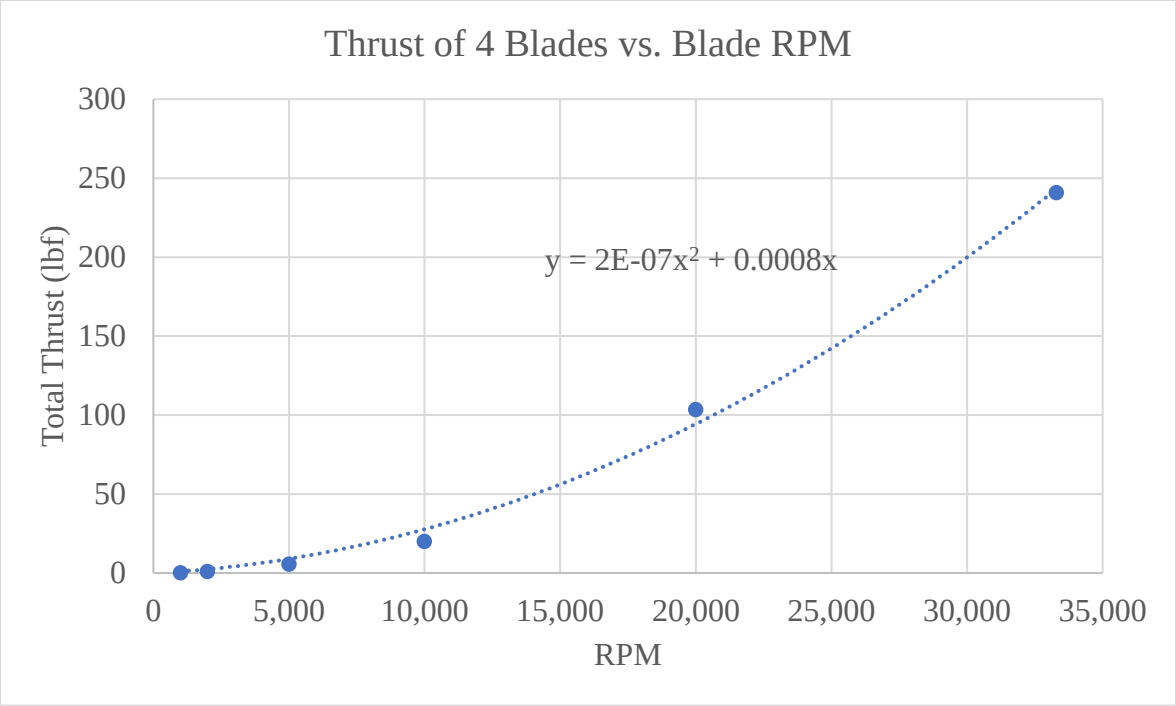

Figure 24: The thrust vs blade RPM (assuming a four bladed quadcopter design)

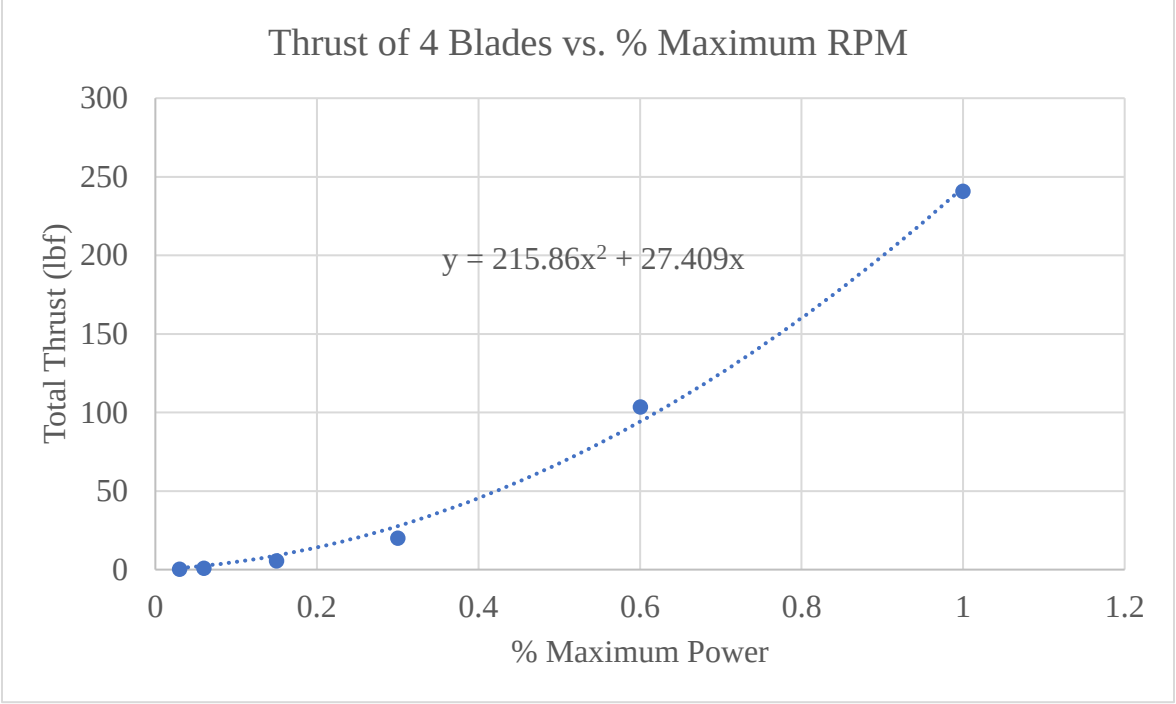

Figure 25: The thrust vs % maximum RPM (assuming a four bladed quadcopter design)

Figure 24 and Figure 25 show the results of the CFD trade study. A polynomial interpolation of the data was done to determine the total thrust as functions of the RPM and % maximum power, respectively.

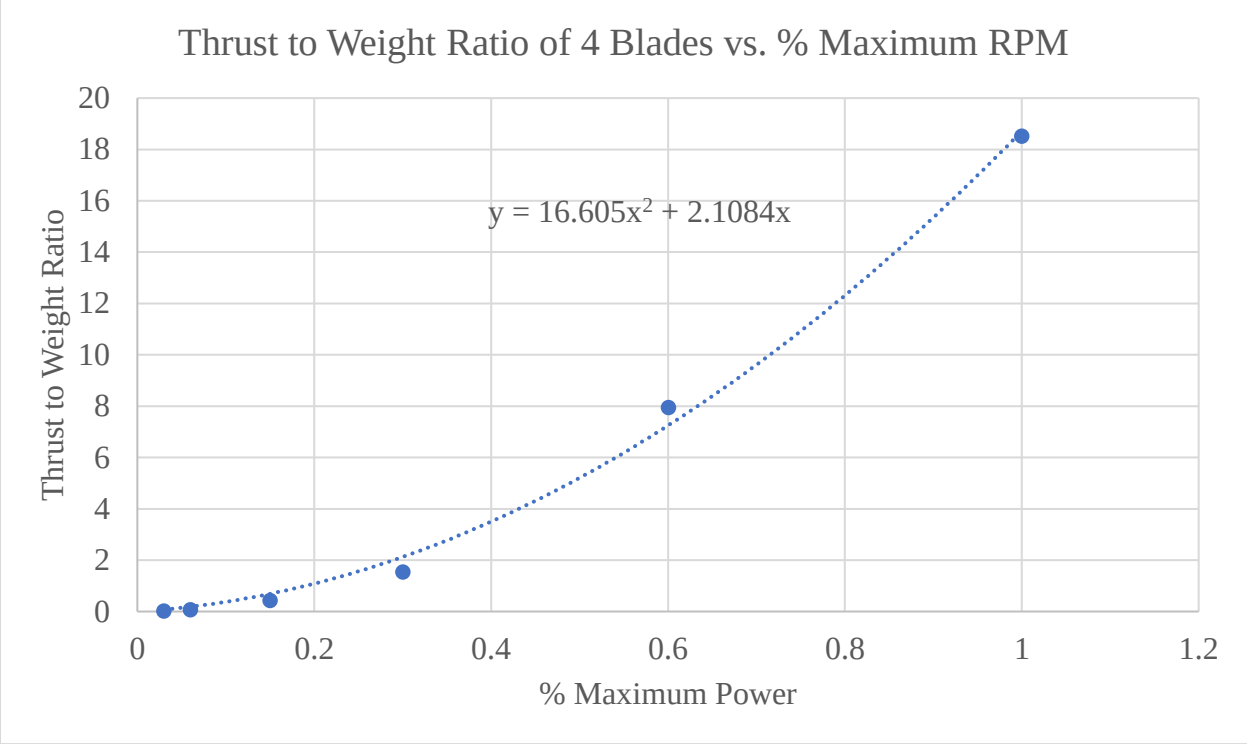

Figure 26: The thrust to weight ratio vs % maximum RPM (assuming a four bladed quadcopter design)

Figure 26 shows the polynomial interpolation of the data to determine the thrust to weight ratio as a function of the % maximum power. This analysis shows that to provide the desired thrust to weight ratio of 3.0, the motors will need to run at 37% power.

This CFD analysis was also done to obtain pressure contours for the FEA analysis of the blade. Figure 27 shows the pressure contours obtained from the max power CFD analysis.

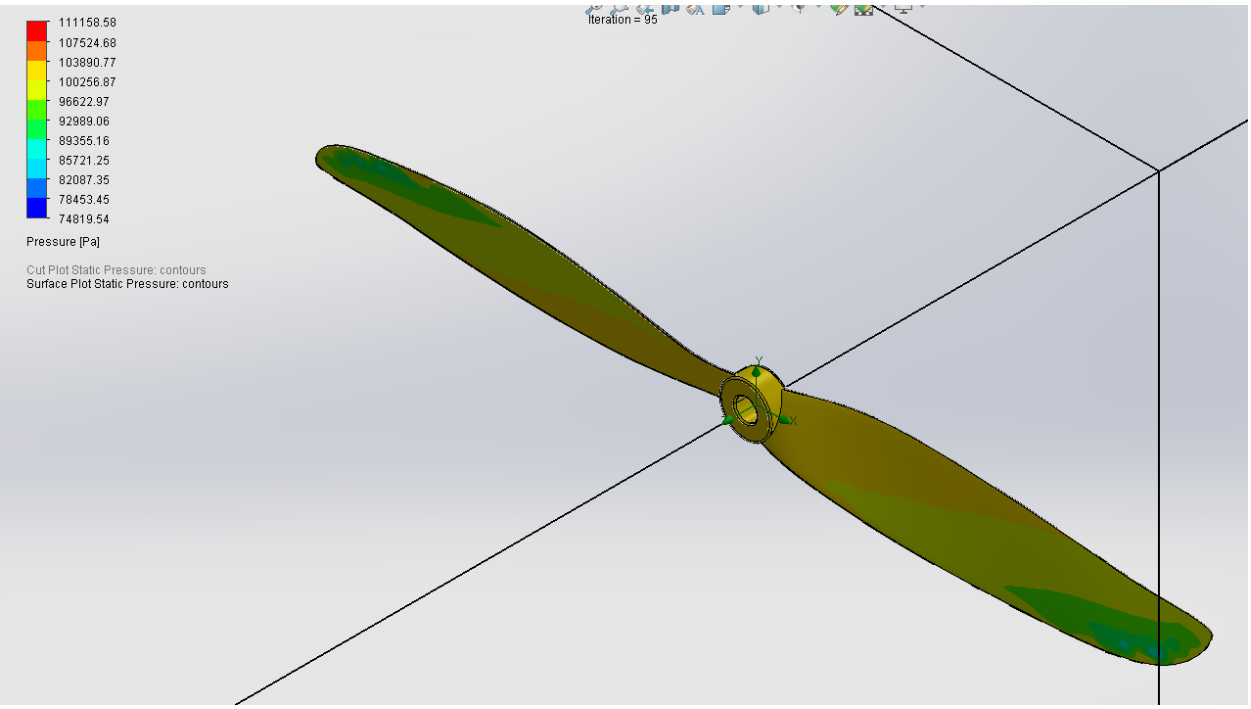

Figure 27: The pressure contours of the blade's CFD analysis

9.1.2: CFD for Drone Body

A CFD analysis was also performed on the body of the drone to assist with the FEA analysis. Specifics of the SOLIDWORKS settings can be found in Appendix A. Figure 28 shows the drone model used for the simulations.

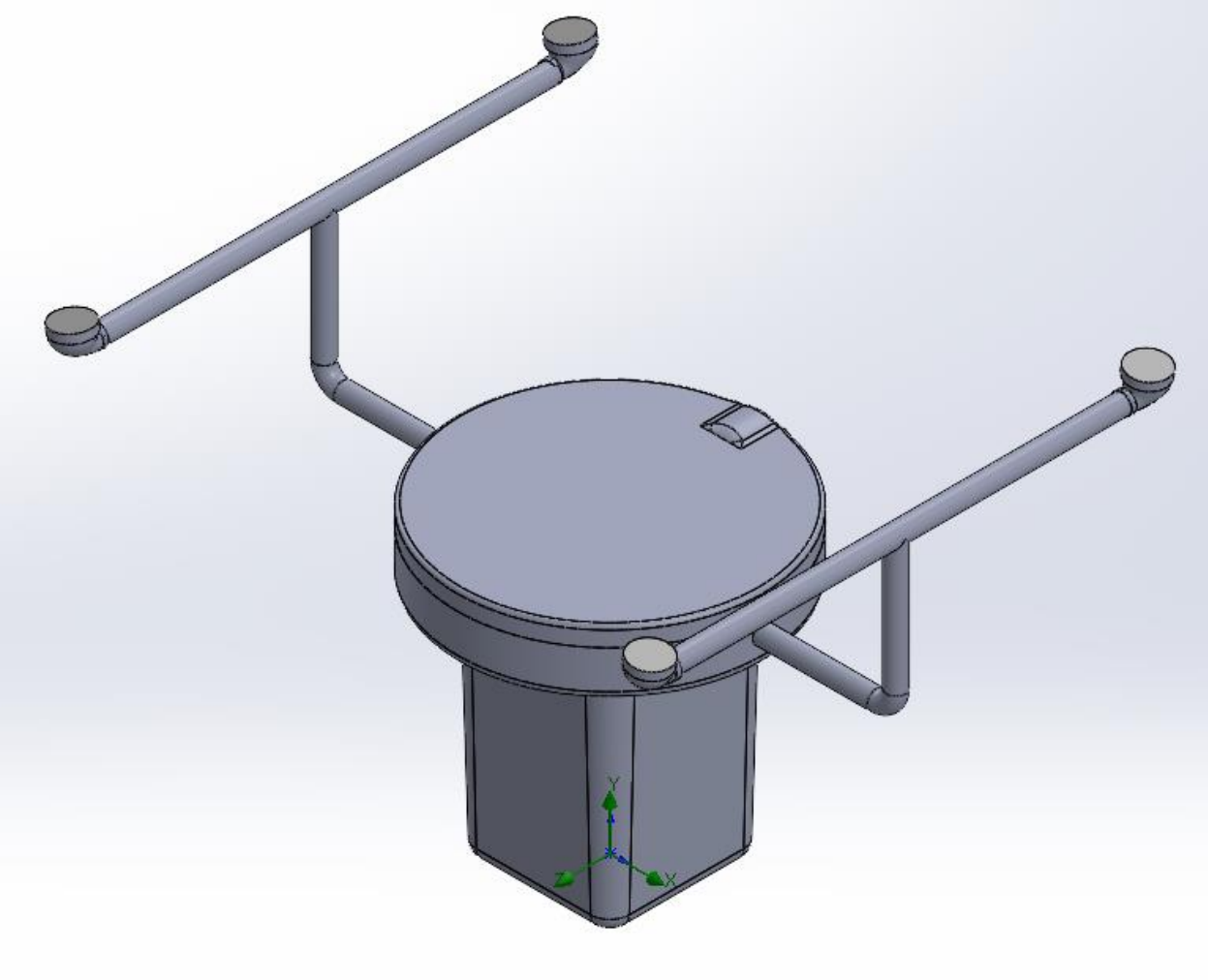

Figure 28: The SOLIDWORKS model of the body of the drone

Figure 29 shows a cut view of the velocity contours of the drone body in flight.

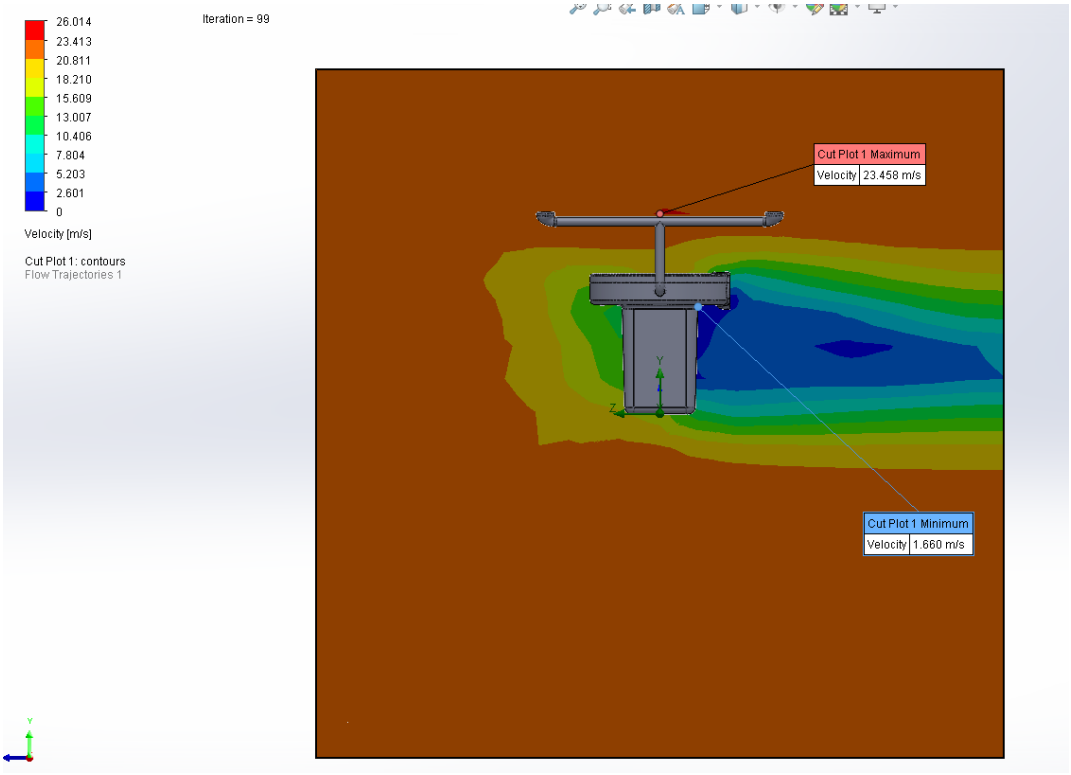

Figure 29: The velocity contours of the body's CFD analysis

Figure 30 shows the pressure contours obtained from the drone body CFD analysis.

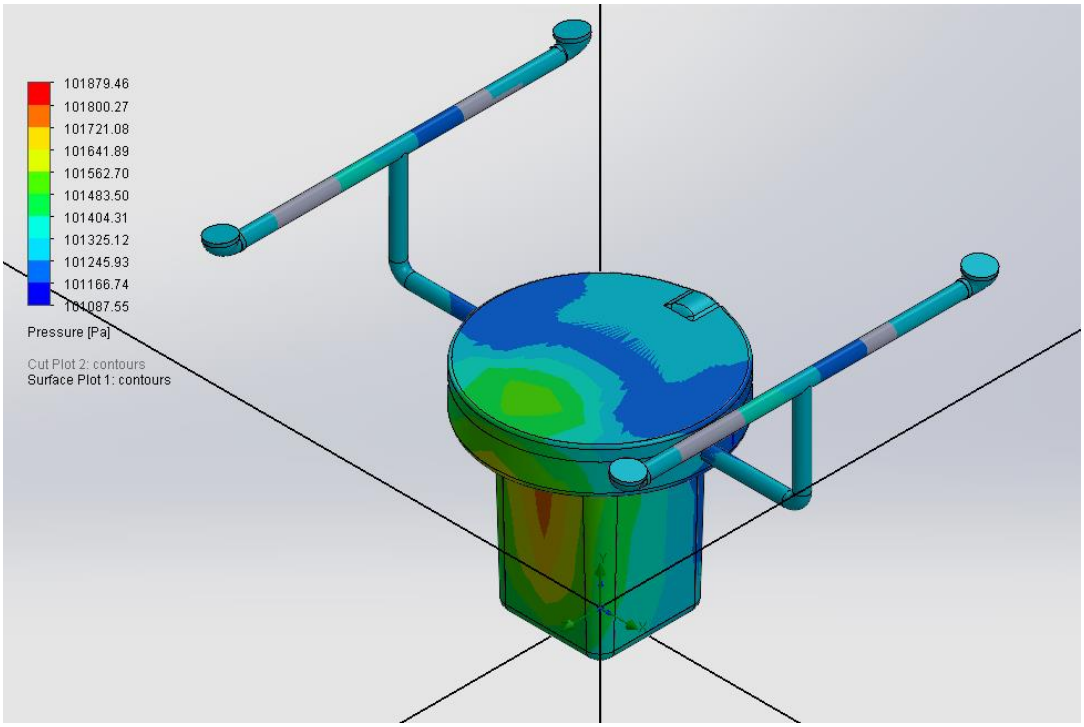

Figure 30: The pressure contours of the body's CFD analysis

A final CFD analysis was done to analyze the flow when the rotors were moving at 100% power. The specifics of this analysis can be found in Appendix A.

Figure 31 shows a cut view of the velocity contours of the drone body in flight. The flow caused by the rotating blades can also be seen.

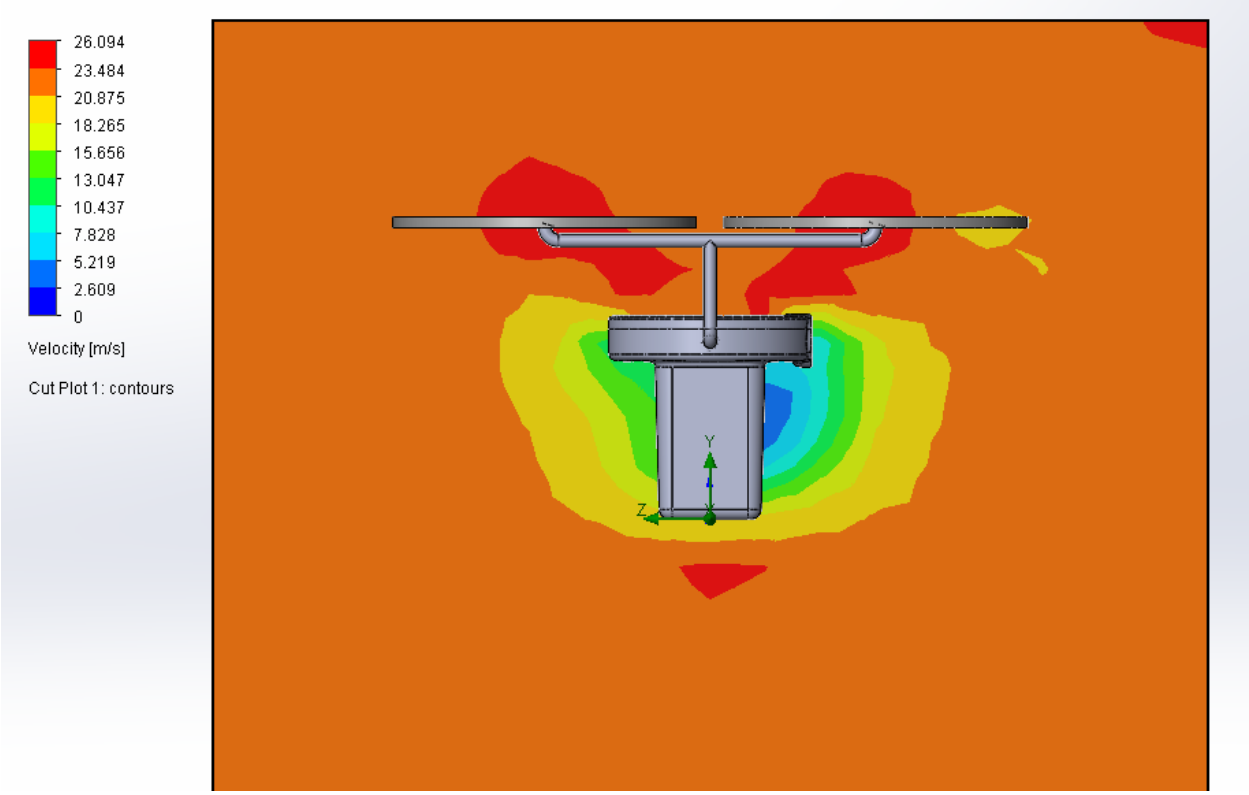

Figure 31: The velocity contours of the body's CFD analysis at full power

Figure 32 shows the pressure profile obtained from the final drone body CFD analysis.

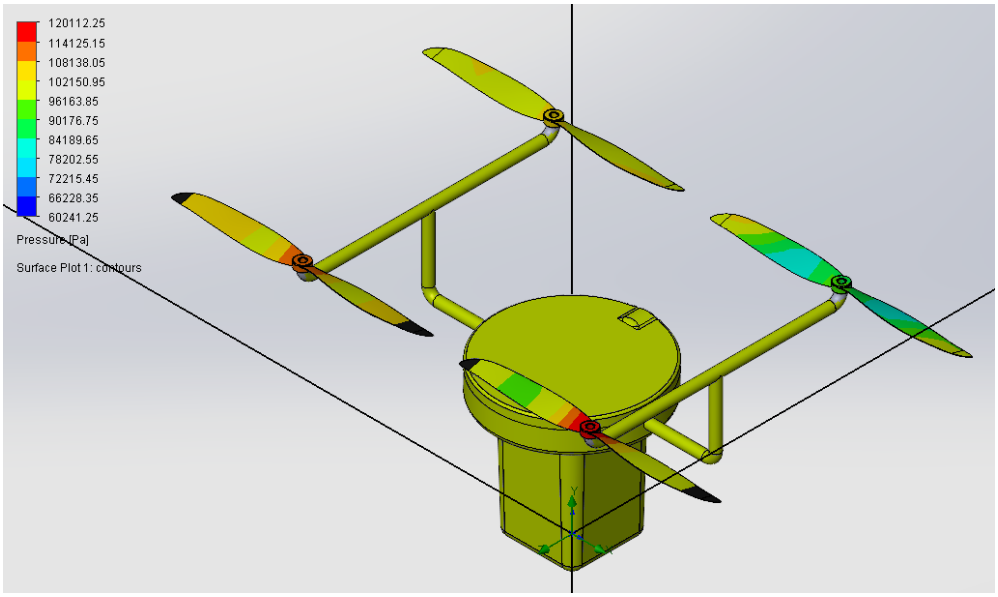

Figure 32: The pressure contours of the body's CFD analysis at full power

A summary of all simulation results can be found in Chapter 12.4: Simulations.

9.2: Finite Element Analysis (FEA)

9.2.1: FEA for Rotor Blades

A finite element analysis was done on the rotor blade to determine if the blade would fail under maximum power conditions (33,300 RPM). The selected material was HexTow AS4 Carbon Fiber.[12] Specifics of the SOLIDWORKS settings can be found in Appendix A.

Figure 33 shows the factor of safety plot from the static stress FEA analysis on the blade.

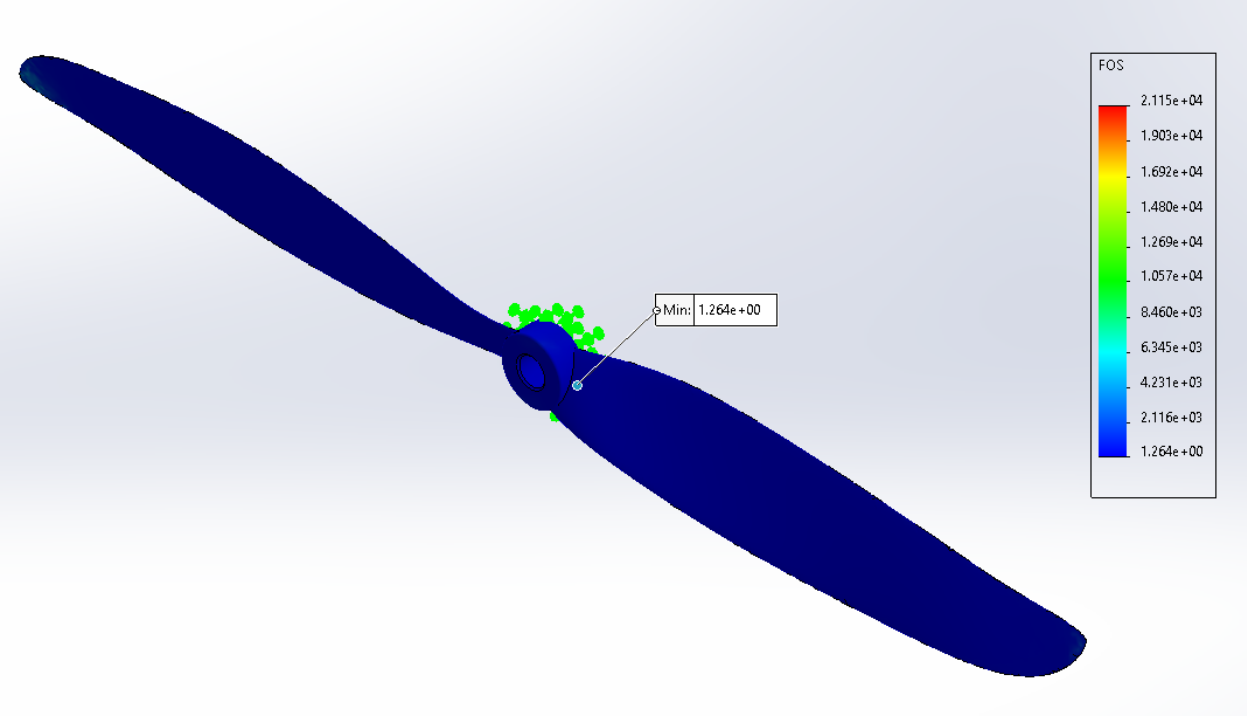

Figure 33: The FOS plot of the blade's FEA analysis

Based on the minimum factor of safety (FOS) of 1.264, it was determined that this blade design and material was satisfactory. The FOS will almost always be higher, as the drone will rarely operate at maximum RPM.

9.2.2: FEA for Drone Body

A finite element analysis was done on the rotor blade to determine if the blade would fail under the specified maximum thrust to weight ratio of 3.0. The selected material was high impact polystyrene.[1213] Specifics of the SOLIDWORKS settings can be found in Appendix A.

Figure 34 shows the factor of safety plot from the static stress FEA analysis on the drone body.

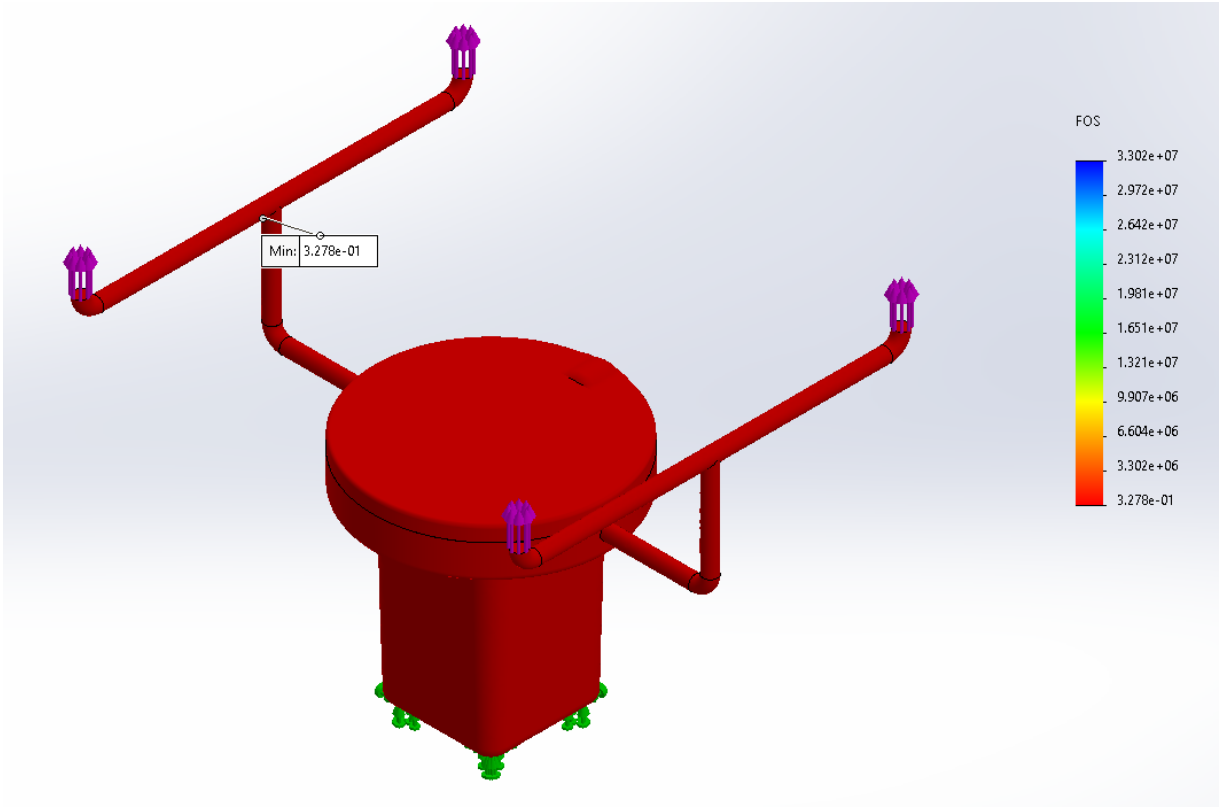

Figure 34: The FOS plot of the body's FEA analysis with high impact polystyrene

Based on the minimum factor of safety (FOS) of 0.3, it was decided that this body design and material was not satisfactory. This analysis was done with a polymer to attempt to save weight, however, the analysis indicates that was not a suitable decision. Further collaboration with the weight sizing team resulted in the decision to try switching to 7075-T6 aluminum.[13] This is a material that has a much higher yield strength than the previously selected polymer, but still has a density low enough to stay within the weight requirements.

Figure 35 shows the factor of safety plot from the static stress FEA analysis on the drone body with updated material selection.

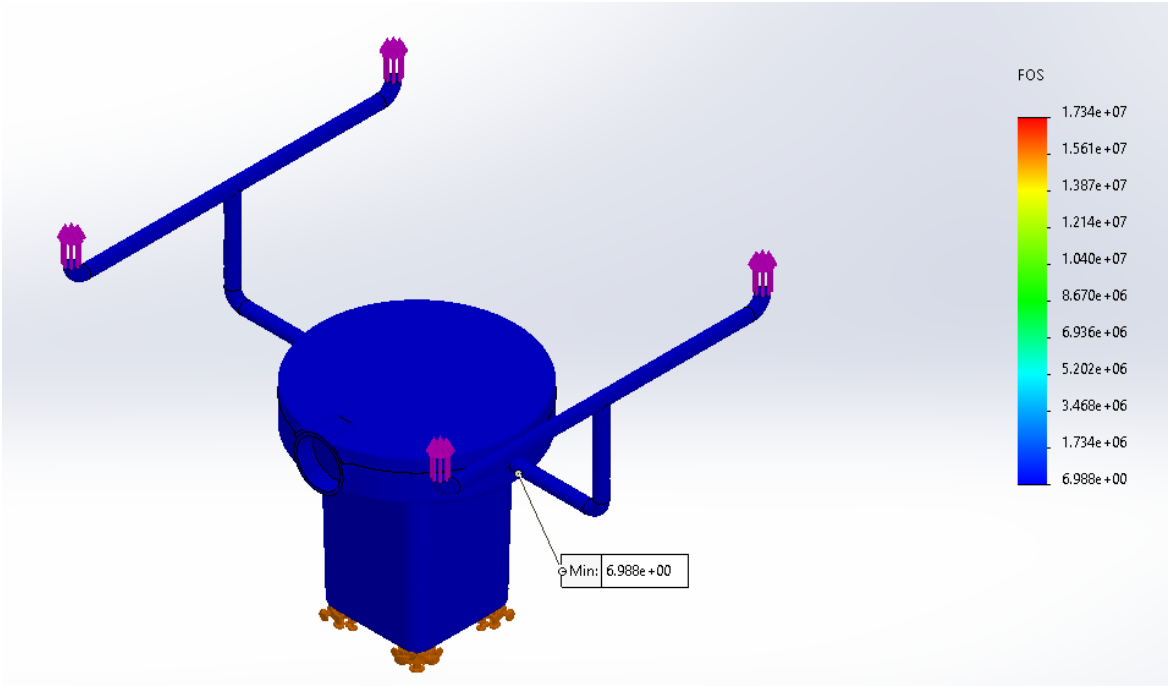

Figure 35: The FOS plot of the body's FEA analysis with 7075-T6 aluminum

This analysis had a minimum factor of safety of 6.988, which indicates that this design is satisfactory for the static analysis. A fatigue analysis was also performed to validate the structural integrity of the design. Specifics of the SOLIDWORKS settings can be found in Appendix A.

Figure 36 shows the cycles to failure for the fatigue stress FEA analysis on the drone body with updated material selection.

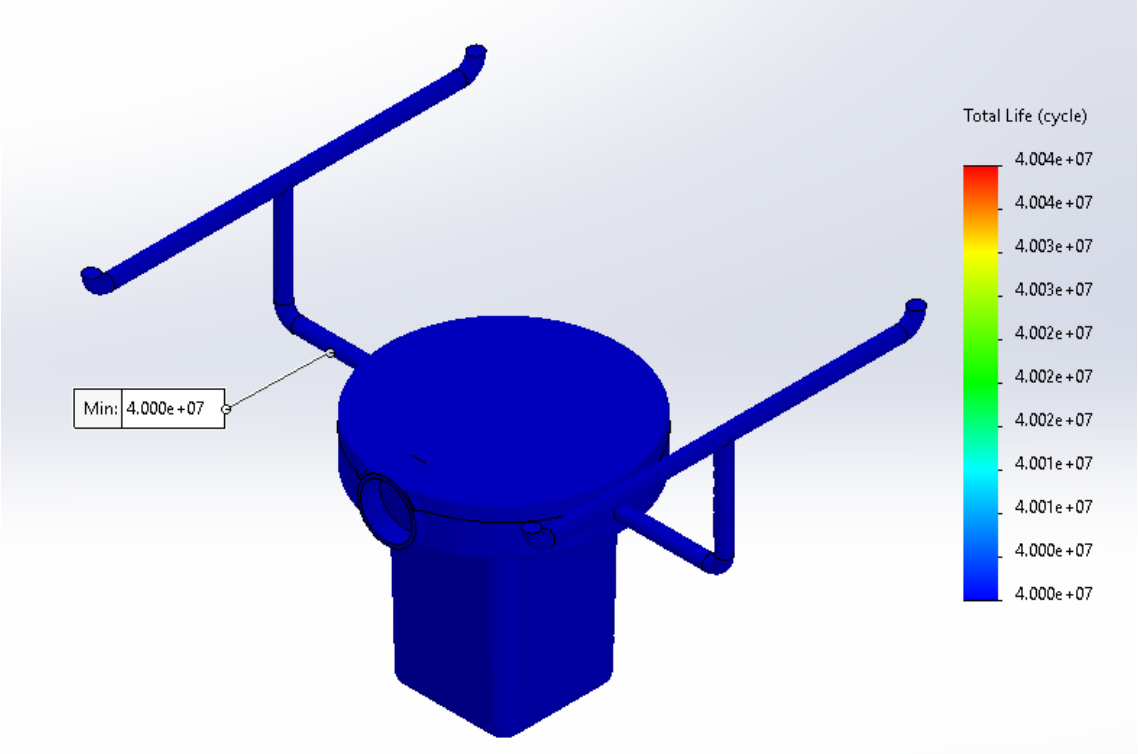

Figure 36: The cycle to failure plot of the body's fatigue analysis with 7075-T6 aluminum

This analysis had a minimum number of cycles to failure of 40,000,000 cycles, which indicates that this design is satisfactory for the fatigue analysis. Therefore, the finite element analysis indicates that this design is satisfactory. The results of this finite element analysis were further confirmed with manual calculations as described in the following section.

9.2.3: Verification of Finite Element Analysis (FEA)

In order to verify and strengthen the results of the finite element analysis, a manual stress analysis was done on the point of maximum stress on the body of the drone. The arms of the drone were analyzed as beams using cantilever beam analysis. Then the factor of safety was found using the distortion energy method to calculate the von mises stress. This von mises stress calculation is the same method of safety factor calculation used in the SOLIDWORKS FEA.

The results of this manual analysis compared to the results of the finite element analysis are presented in Table 8. The full details of this manual analysis can be found in Appendix B.

Table 8: Comparison of minimum factor of safeties of FEA and manual stress analyses

Minimum static factor of safety (FEA):	6.99
Minimum static factor of safety (manual):	6.80
% Difference	2.76%

Based on the low % difference between the two analytical methods, it is the opinion of the Kennesaw State University engineering team that the FEA analysis provides results are acceptable for this analysis.

Fatigue analysis is a complicated problem with several different ways of obtaining a result. For this verification analysis, the stress-life method was used. Based on the maximum stress acting on the drone, it is estimated with the stress-life method that the material will fail at 400,000,000 cycles. While the FEA and manual calculations are off by a large amount, it is still believed that the FEA analysis is accurate. The fatigue properties of aluminum are often not well defined, which makes hand fatigue calculations for aluminum very imprecise, as techniques more precise that the stress-life method require a large degree of estimation.[28] Additionally, since both methods indicate a very high cycles to failure, both fatigue analyses indicate that the design is satisfactory.

A summary of all simulation results can be found in Chapter 12.4: Simulations.

[28] Budnyas and Nisbett, *Shigley's Mechanical Engineering Design*. 10th. New York: McGraw Hill Education.

Chapter 10: Bill of Materials

Table 9: Bill of materials for one unit of the SAUSER project

COMPONENT	MAKE/BUY	QUANTITY	PRICE
Dock Shell	MAKE	1	15
Body	MAKE	1	50
Jetson Nano	BUY	1	59
Pixhawk	BUY	1	94.99
iFlight Succex-E	BUY	1	41.99
iFlight 4pcs 2208 2450kv	BUY	1	91.99
Turnigy 14.8v 5Ah	BUY	4	37.18
GoPro Hero 9	BUY	1	445.99
OC-110	BUY	1	30
RC-100	BUY	1	20
TC-200	BUY	1	25
TR-110	BUY	1	75
		TOTAL	1097.68

Table 9 shows all the parts necessary for the drone body as well as whether the parts need to be manufactured or purchased. All prices are in USD.

Chapter 11: Economic Analysis

Error! Reference source not found. outlines the initial cost of the SAUSER system. T he costs of manufacturing were estimated with the numbers described in the literature review. Some estimations are made (e.g. man hours and hourly for mount installation) to get an estimation of the initial cost. An additional $500 of assembly cost was also added for each drone to account for the cost of assembly and other miscellaneous manufacturing and distribution costs.

Table 10: Initial cost of the SAUSER system

Initial Cost	
Total Drones in System	40
Drone and Mount OTS Cost (per unit)	$1,100
Estimated Drone Machining Cost (per unit)	$15
Estimated Drone Assembling and Delivery Cost (per unit)	$500
Initial Drone Cost (per unit)	$1,615
Initial Drone Cost (per system)	**$64,600**
Estimated Mount Installation Hours (per unit)	20
Mount Installation Cost (per unit per hour)	$100
Total Mount Installation Cost (per unit)	$2,000
Total Mount Installation Cost (per system)	**$80,000**
Estimated Design Hours	288
Engineering Design Cost (per hour)	$150
Total Engineering Design Cost	**$43,200**
Total Initial Cost (per system)	**$187,800**

Table 11 outlines the annual cost of the SAUSER system. The drone operator and server costs were estimated with the numbers described in the literature review. Some estimations were made (man hours and hourly rate for maintenance) to get an estimation of the annual cost.

Table 11: Annual cost of the SAUSER system

Annual Costs	
Total Drones in System	40
Power Consumption (kW per charge)	0.30
Power Cost (per kWh)	$0.10
Power Cost (per charge)	$0.03
Estimated Number of Charges (per year)	25
Power Cost (per unit per year)	$0.74
Power Cost (per system per year)	**$29.60**
Maintenance (hour per unit per year)	2
Maintenance Cost (per hour)	$100
Maintenance Cost (per year)	$200
Maintenance Cost (per system per year)	**$8,000**
Server Cost (per year)	**$38,892**
Drone Operator Salary (per operator per year)	$48,931
Total Drone Operator Employee Cost (per operator per year)	$68,503
Estimated Operators Required	6
Total Drone Operator Cost (per system per year)	**$411,020**
Total Annual Cost (per system)	**$457,942.00**

To evaluate if the SAUSER project fits within the specified budget, a present value analysis was performed. The result of this analysis is in **Error! Reference source not found.**.

Table 12: Present value analysis of the SAUSER system

Present Value Analysis	
Total Initial Cost (per system)	$187,800
Total Annual Cost (per system)	$457,942
Present Value (assuming 5% interest for 10 years)	$3,723,907

Based on this analysis, the SAUSER project fits within the project budget. Therefore, it is the opinion of the Kennesaw State University team that the SAUSER project is economically viable.

Chapter 12: Results and Discussion

12.1: Electronics

The physical capacity for the drone is limited, so the largest batteries that can fit were chosen. Four 5 Amp hour batteries were able to fit in the chassis of the drone. This gives the drone 20 Amp hours at a max voltage of 16 volts, or 320 Watt hours of power. Lithium batteries are not made to drain to lower than a certain threshold. The discharge percentage will be 80%; leaving 20% left when the battery will need to be charged. This is for battery life maintenance. Using these parameters and motor information, the flight time on 20 Ah battery capacity is 34.4 minutes at 50% throttle. Figure 53 in Appendix G shows the motor information used for battery capacity calculations. Calculations for battery capacity can be found in Figure 54. This does not currently fit the original design criteria, but it does open the project to solutions for the future.

Possible other battery solutions include the Turnigy 6.6 Ah battery. This would increase the flight time to 45.4 minutes. The drone body would need slight modification to accept these larger batteries. This is a possible upgrade for the line of drones. A custom battery could also be commissioned that optimizes space. A soft cell battery, like in cellphones and laptops, can be used to give a required capacity and take up a specific volume of the chassis. The Turnigy battery was chosen because there are variants of the battery with higher capacities, but they do not fit in the drone model. The SAUSER would have to be redesigned to accept larger batteries and higher weights. A possible solution is a more energy dense battery chemistry. The 5 Ah batteries stayed under the max weight of the drone, but there are batteries in development that can provide more energy at similar weight. Those batteries are not as easily accessible though.

The Wibotic equipment specified in Chapter 5 will need coordination with the company. When the SAUSER enters production, Wibotic will be a major vendor and ally for producing the drone. This would give more accurate information on charging and pricing. There are not any pricing details on Wibotic’s website because they quote buyers on product solutions.

12.2: Sizing

Table 13 describes the results and knowledge gained from the sizing analysis.

Table 13: Summary of the Sizing section results.

Sizing	**Result**
Chapter 6	• The sizing analysis to account for the mass and weight of individual components and modules obtained. • Mass of the in-house designed parts accounted using SolidWorks mass properties tool. • Combination of aluminum 7075-T6 and carbon fiber Hexcel AS4C 3k used to achieve desired sizing goal. • Payload capacity of 2 lbf as sought under design goal achieved. • MTOW was determined to be 13.108 lbf compared to design goal of 13.00 lbf.

12.3: Rotor Design and BEMT analysis

Table 14 describes the results and knowledge gained from the rotor design analysis.

Table 14: Summary of the rotor blade section.

Rotor Design Section	**Results**
Chapter 7	• Initial assessment of the material selection for rotor blade with structural strength to withstand forces when in flight. • Hexcel AS4C 3k carbon fiber as the selected material for blades with tensile strength of 685k psi. • Physical dimension of rotor with radius being 167.01 mm and rotor hub diameter measuring 9 mm. • Rotor blade twist of 7.25 degree to approximate uniform lift generation along its profile.

Table 15 describes the results and knowledge gained from the BEMT analysis.

Table 15: Summary of the BEMT analysis results.

BEMT Analysis	**Result**
Chapter 8.2: Rotor Design Power for Single Rotor	• BEMT analysis to determine the design power of a single rotor accomplished. • Parametric values calculated to determine the performance of the drone when in hover. • Single rotor thrust of 14.441 N and total thrust of 57.764 N validate the hover capabilities with MTOW. • Total Power consumption of 133.79 W validates the drone flight time as per design goals is accomplished. • The parametric values of SAUSER confirm better results compared to the similar drone (DJI Inspire 2) used for benchmarking.

12.4: Simulations

Table 16 describes the results and knowledge gained from each simulation.

Table 16: Summary of CFD/FEA results

Simulation Section	**Results**
Chapter 9.1.1: CFD for Rotor Blades	• Initial assessment of aerodynamic qualities of rotor blades. Assessment indicated that the rotor blades are capable of providing sufficient thrust for the selected brushless motors. • Pressure contours obtained for the maximum motor power. These results were then exported for Chapter 9.2.1: FEA for Rotor Blades.
Chapter 9.1.2: CFD for Drone Body	• Initial assessment of aerodynamic qualities of drone body. Velocity and pressure profiles obtained. • Initial assessment of aerodynamic qualities of drone body with four spinning rotors. Velocity and pressure profiles obtained. • Pressure contours obtained for the body. These results were then exported for Chapter 9.2.2: FEA for Drone Body.
Chapter 9.2.1: FEA for Rotor Blades	• Factor of safety for static analysis of blade spinning at maximum power obtained. • Design of rotor blade and material selected determined to be satisfactory.
Chapter 9.2.2: FEA for Drone Body	• Factor of safety for static analysis of done body obtained. • Number of cycles to failure for drone body obtained. • Design of body determined to be satisfactory. • Material of body (polymer) determined to be unsatisfactory. A new material was selected (7075-T6 aluminum) and found to be satisfactory.
Chapter 9.2.3: Verification of Finite Element Analysis (FEA)	• Hand calculations indicated that the FEA produced accurate results.

12.5: Economic Analysis

The economic analysis has indicated that this project is within the budget specified in Chapter 3.7: Budget. It is the opinion of the Kennesaw State University engineering team that this is an economically viable project.

Chapter 13: Conclusions

The KSU team's final recommendations for the project are listed below:

- The use of carbon fiber for the rotor blades is necessary if the drone is to operate at or near maximum power. If a different material is desired, the blades may be unable to safely operate at maximum power.
- The sizing analysis indicates that the SAUSER has an overall weight of 13.108 lbf. while achieving the desired payload capacity and capability to house all desired electronics needed for flight and surveillance.
- The BEMT analysis indicates that the SAUSER produces required thrust at MTOW and achieve a flight time of 34 minutes compared to design goal of 45 minutes.
- The electronic analysis indicates that further development needs to be done, software wise, to maintain proper battery life. Larger capacity batteries and higher energy densities are favorable.
- The electronic analysis also supports that the idea of a wirelessly charged drone and a wireless area network for drone control is possible. This subject can be taken to software engineers and teams with expertise in autonomous vehicles to further develop the system.
- The stress analysis indicates that the drone has a design that will allow the drone to have a large degree of longevity during its service life.
- The economic analysis indicates that the drone fits within the budgetary set at the beginning of the project design process.

Appendix A: CFD and FEA Settings

Appendix A.1: CFD Settings

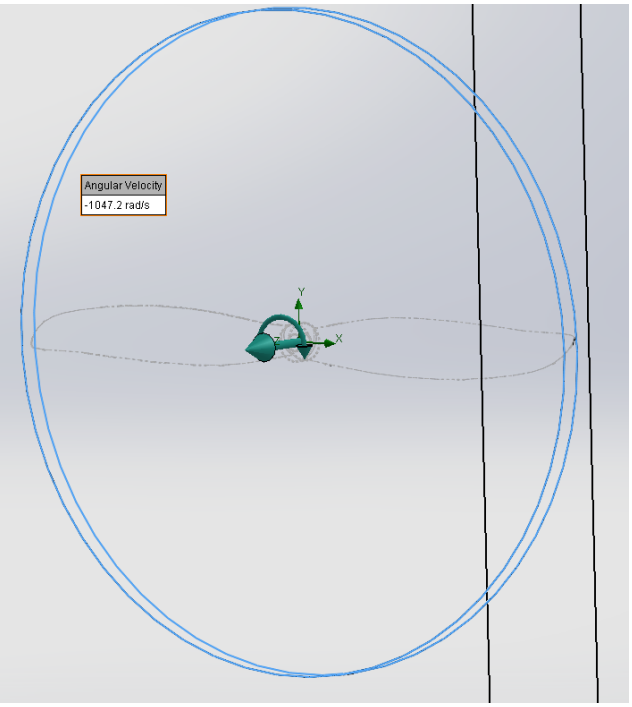

Figure 37: The rotational region of the blade analysis

Figure 37 show the rotational region created in SOLIDWORKS to simulate the rotation of the blade.

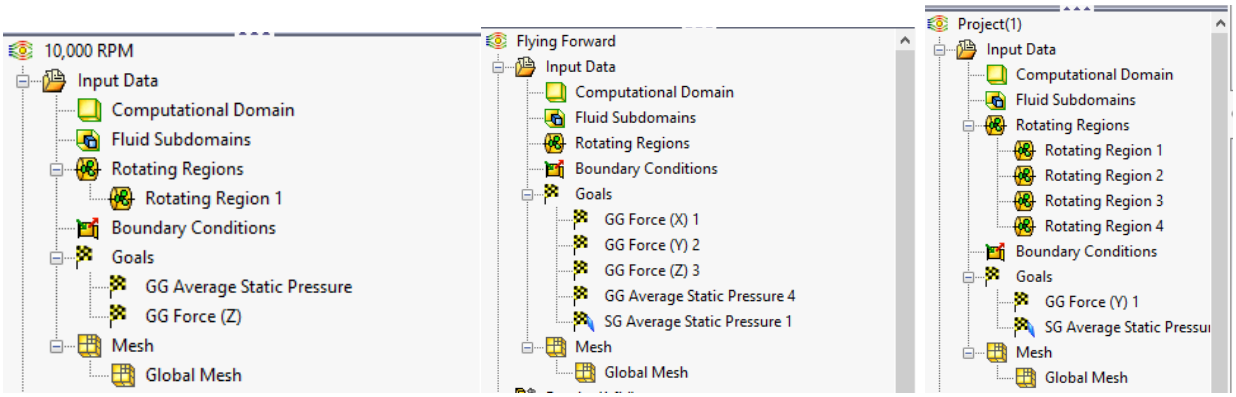

(a) (b) (c)

Figure 38: The boundary conditions for the (a) rotor blade analysis, the (b) drone structure analysis, and (c) full power analysis

Figure 38 shows the rotating region and goal requirements for the various CFD analyses.

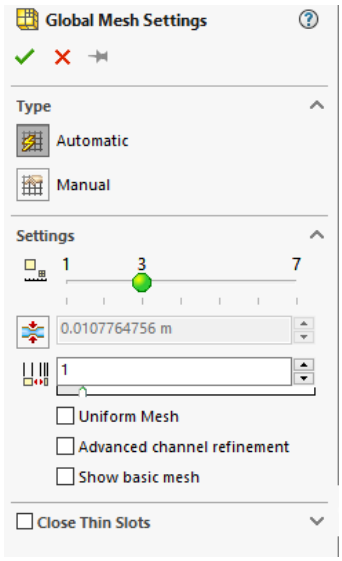

Figure 39: The mesh settings used for the CFD analyses. The mesh density was chosen at the last setting which had a significant effect on the results of the simulation.

Figure 39 shows the SOLIDWORKS mesh settings used to perform the CFD analyses. The automatic mesh was selected for its simplicity and ease of mesh density variation.

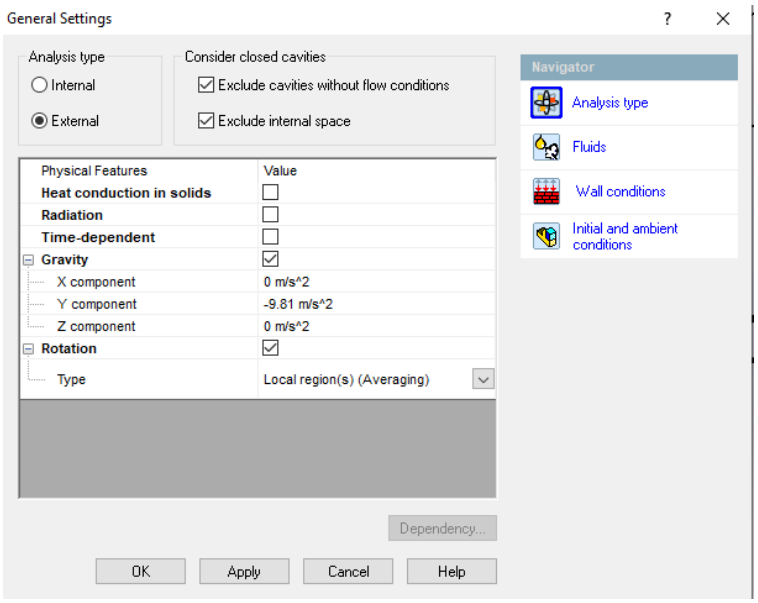
General Settings
Analysis type
Internal
External
Consider closed cavities
Exclude cavities without flow conditions
Exclude internal space
Physical Features
Value
Heat conduction in solids
Radiation
Time-dependent
Gravity
X component
0 m/s^2
Y component
-9.81 m/s^2
Z component
0 m/s^2
Rotation
Type
Local region(s) (Averaging)
Dependency...
OK
Apply
Cancel
Help
Navigator
Analysis type
Fluids
Wall conditions
Initial and ambient conditions

(a)

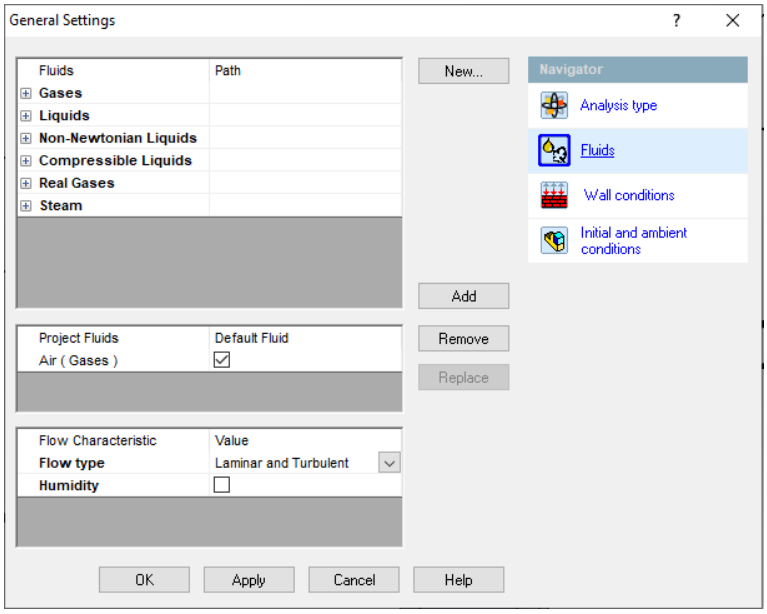
General Settings
Fluids
Path
Gases
Liquids
Non-Newtonian Liquids
Compressible Liquids
Real Gases
Steam
New...
Add
Remove
Replace
Project Fluids
Default Fluid
Air (Gases)
Flow Characteristic
Value
Flow type
Laminar and Turbulent
Humidity
OK
Apply
Cancel
Help
Navigator
Analysis type
Fluids
Wall conditions
Initial and ambient conditions

(b)

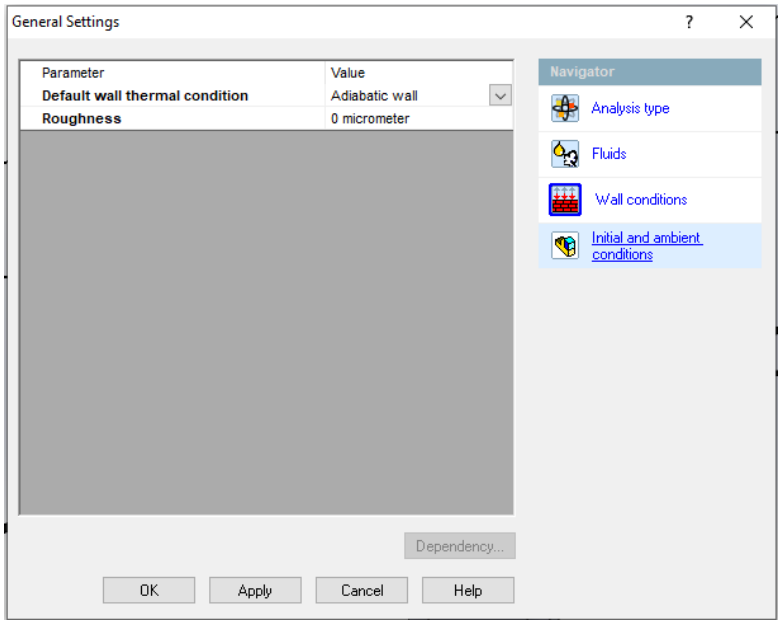
General Settings
Parameter
Value
Default wall thermal condition
Adiabatic wall
Roughness
0 micrometer
Navigator
Analysis type
Fluids
Wall conditions
Initial and ambient conditions
Dependency...
OK
Apply
Cancel
Help

(c)

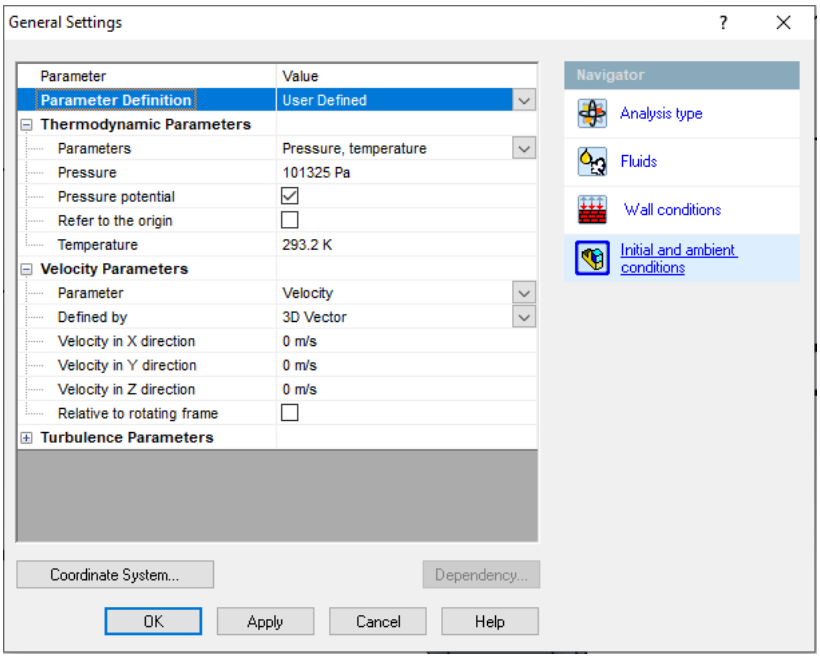
General Settings
Parameter
Value
Parameter Definition
User Defined
Thermodynamic Parameters
Parameters
Pressure, temperature
Pressure
101325 Pa
Pressure potential
Refer to the origin
Temperature
293.2 K
Velocity Parameters
Parameter
Velocity
Defined by
3D Vector
Velocity in X direction
0 m/s
Velocity in Y direction
0 m/s
Velocity in Z direction
0 m/s
Relative to rotating frame
Turbulence Parameters
Navigator
Analysis type
Fluids
Wall conditions
Initial and ambient conditions
Coordinate System...
Dependency...
OK
Apply
Cancel
Help

(d)

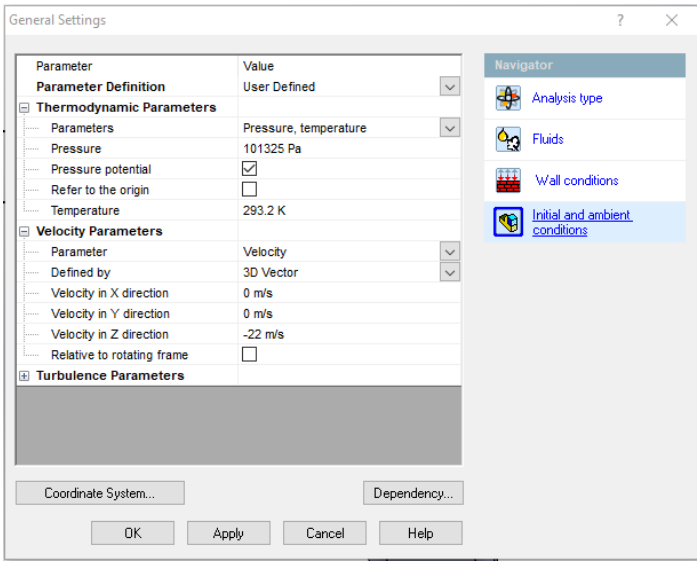

(e)

Figure 40: The (a) general flow settings, (b) selected fluid, (c) wall conditions, (d) initial conditions for the blade analysis, and the (e) initial conditions for the drone structure flow analysis

Figure 40 (a) show the external flow and gravity conditions used in the simulation. Figure 40 (b) shows the selection of air as the working fluid for the simulation. Figure 40 (c) show the simulation wall conditions. Figure 40 (d) shows the ambient and external flow conditions for the blade analysis. Figure 40 (e) shows the ambient and external flow conditions for the body analysis.

Appendix A.2: FEA Settings

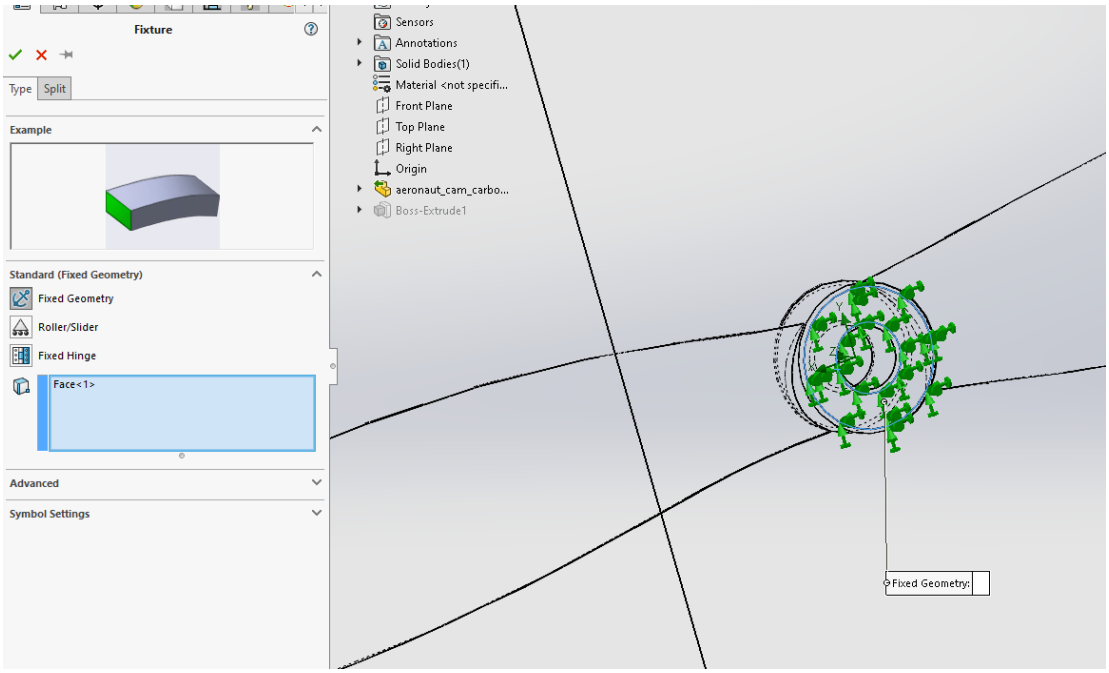

Figure 41: The fixed geometry (green arrows) for the FEA analysis of the blade

Figure 41 shows the fixed geometry boundary condition for the blade FEA. This models the blade being attached to the drone body by the motor.

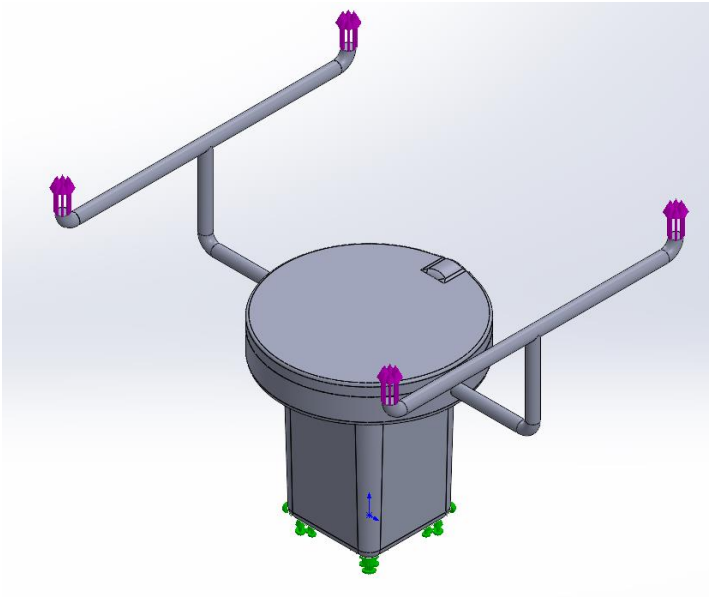

Figure 42: The lifting forces (purple arrows) and the fixed geometry (green arrows) for the FEA analysis of the drone structure

Figure 42 shows the fixed geometry and lifting force boundary conditions for the drone body FEA. These model the gravitational forces and lift provided by the blades, respectively.,

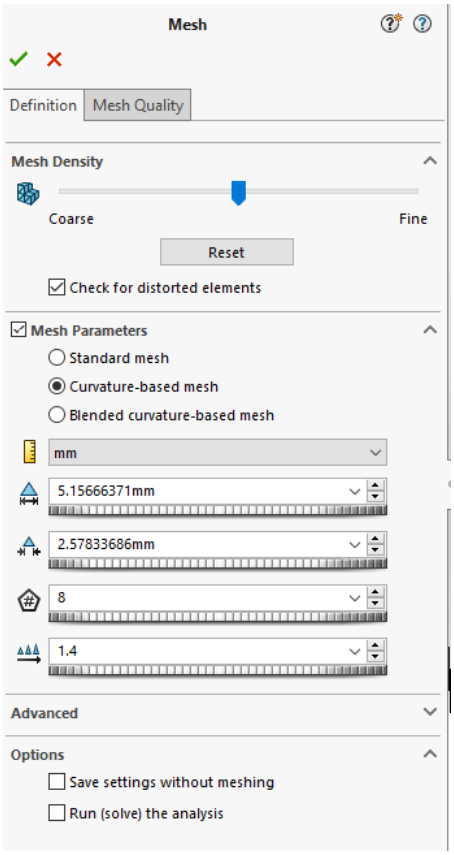

Figure 43: The mesh settings used for the FEA analyses. The mesh density was chosen at the last setting which had a significant effect on the results of the simulation.

Figure 43 shows the SOLIDWORKS mesh settings used to perform the FEA analyses. The curvature-based mesh was selected to account for the curvature of the blades and drone body.

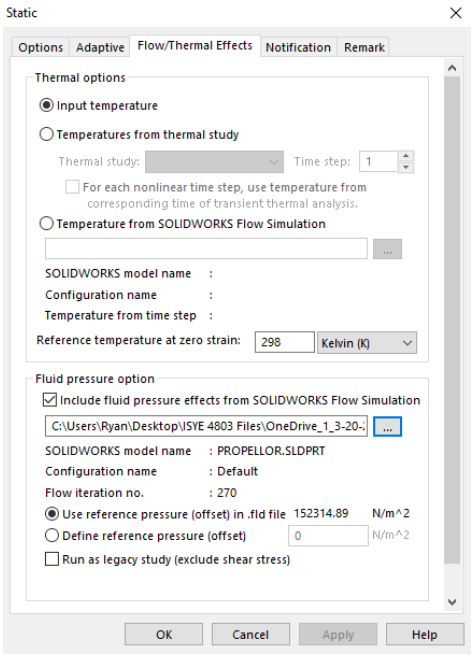

Figure 44: The settings used to import CFD results into FEA boundary conditions

Figure 44 shows the technique used to import the pressure profiles of the CFD analyses into the FEA analyses.

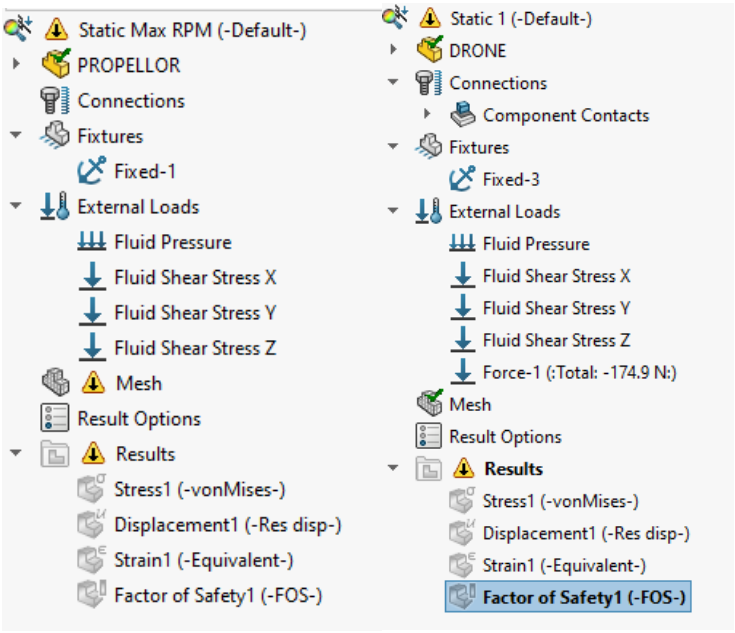

(a) (b)

Figure 45: The boundary conditions for the (a) rotor blade analysis and the (b) drone body static analysis

Figure 45 shows the fixed geometry, the component contacts, and external loads (fluid pressure, fluid shear stress, and external forces) boundary conditions for the FEA analyses. Figure 45 (a) is for the blade analysis and Figure 45 (b) is for the drone body analysis.

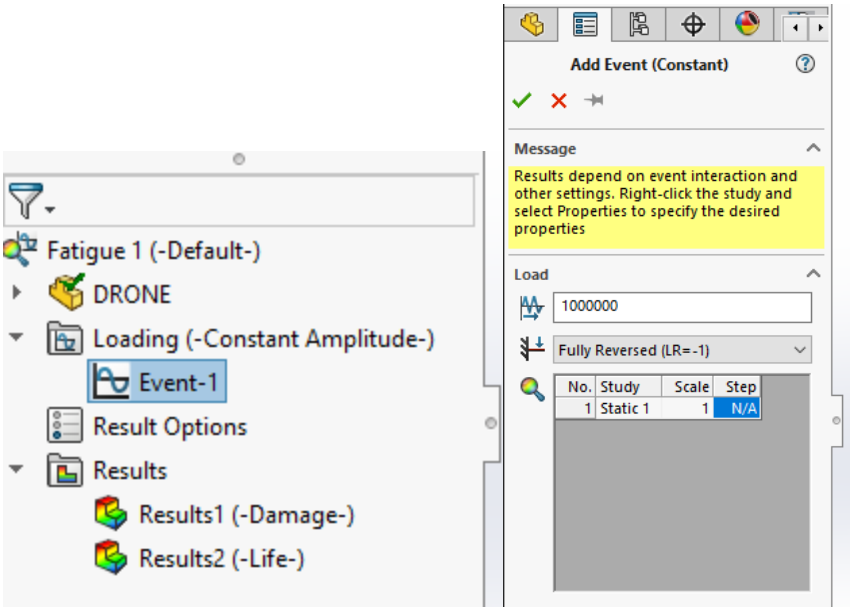

(a) (b)

Figure 46: The settings used to import static FEA results into the fatigue FEA analysis

Figure 46 shows the technique used to import the static stress results into the fatigue stress study.

Appendix B: Manual Verification of Computational Methods

Appendix B.1: Static Analysis

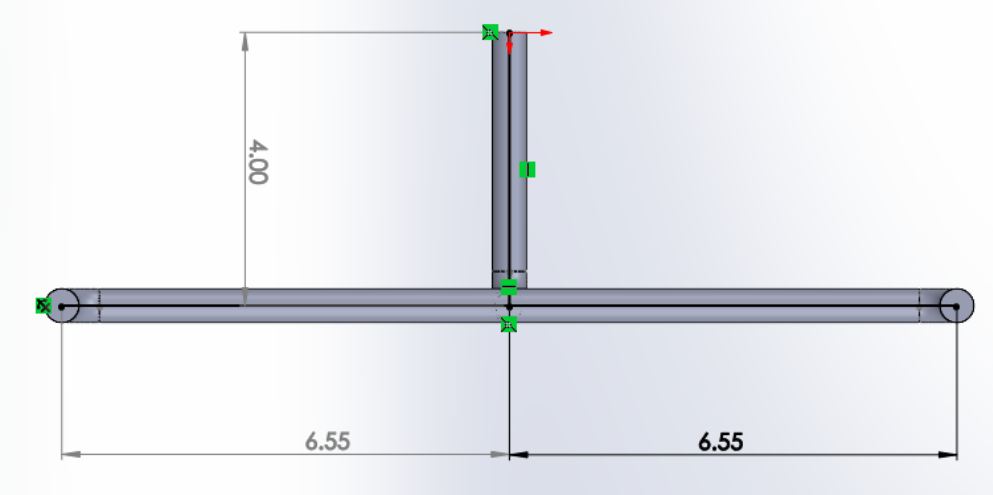

Figure 47: The drone arms (measurements are in inches)

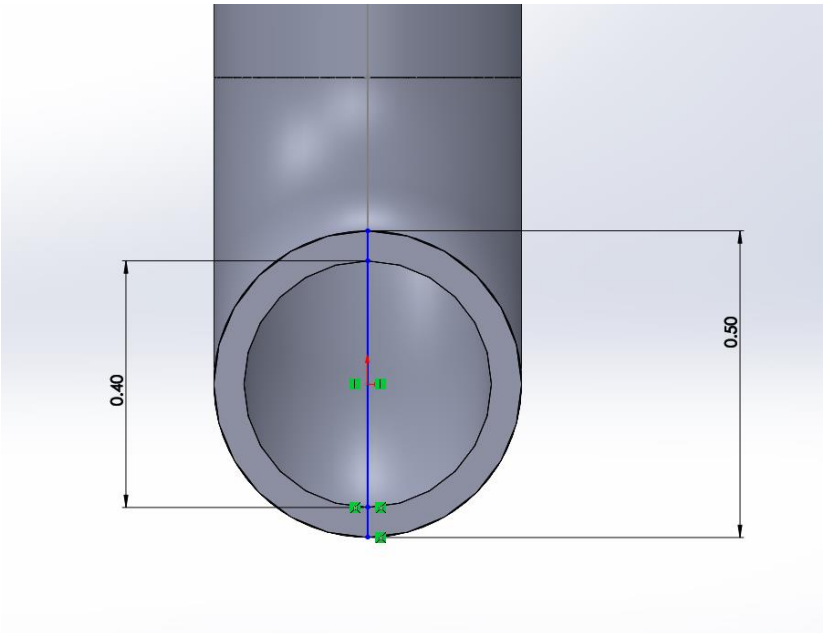

Figure 48: The hollow tube cross section of the drone arms at the point of maximum stress. The point of highest stress is located at the lowest point in the cross section (measurements are in inches)

Figure 47 shows the geometry of the arms (the point of maximum stress is at the red origin). The transverse shear force acting on cross section containing the point of maximum stress was calculated using the following equation.[28] The cross section of this point is shown on Figure 48.

$$\mathrm{F} = 0.5 * \frac{\mathrm{T}}{\mathrm{W}} * \mathrm{W} = 0.5 * 3 * 13\ \mathrm{lbf} = 19.5\ \mathrm{lbf}$$

F = transverse shear force acting on cross section

T/W = specified thrust to weigh ratio

W = total takeoff weight

Note that the total force is multiplied by 0.5 because the drone features two such arms, so each arm only holds half the total load.

The moment acting on cross section containing the point of maximum stress was calculated using the following equation.[28]

$$\mathrm{M} = \mathrm{F} * \mathrm{L} = 19.5\ \mathrm{lbf} * 4\ \mathrm{in}\ =\ 78.0\ \mathrm{lbf} * \mathrm{in}$$

M = moment acting on cross section

L = the normal distance from the cross section of the

The stress caused by the transverse shear stress is 0 because the point of maximum stress is on an outer surface of the arm.[28] Therefore, the only stress component acting on the maximum stress point is the normal stress caused by the moment. This stress was calculated using the following equation.[28]

$$\sigma_{\mathrm{x}} = \frac{-M * \mathrm{y}}{\mathrm{I}} = \frac{-(78.0\ \mathrm{lbf} * \mathrm{in}) * (0.25\ \mathrm{in})}{(\pi/64)(((0.\ \mathrm{in})^4} = 10765.6\ psi$$

σ_x = the normal stress acting on the point of maximum stress in the x direction

y = the normal distance from the neutral axis to the point of maximum stress

I = the second moment of area of the cross section

Finally, the factor of safety for this stress was found with the following equation.[28]

$$n = \frac{S_y}{\sqrt{\sigma_x^2 - \sigma_x\sigma_y - \sigma_y^2 + 3\tau_{xy}^2}} = \frac{73224\ psi}{\sqrt{(10765.6psi)^2}} = 6.80$$

σ_y = the normal stress acting on the point of maximum stress in the y direction

τ_{xy} = the shear stress acting on the point of maximum stress

S_y = the material's yield strength[13]

Appendix B.2: Fatigue Analysis

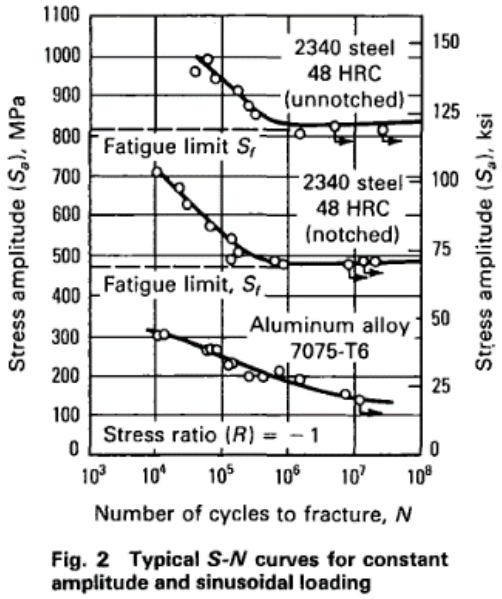

Fig. 2 Typical *S-N* curves for constant amplitude and sinusoidal loading

Figure 49: The stress life diagram for 7075-T6 aluminum.[29]

Figure 49 shows the fatigue stress performance for 7075-T6 aluminum used for the manual verification of the FEA analysis. For the stress-life method, the number of cycles to fracture is obtained by reading the S-N curve for 7075-T6 aluminum. The maximum stress (10765.6 psi) for this fully reversed cyclic loading is used to find the cycles to fracture.[28]

[29] ASM International, *Elements of Metallurgy and Engineering Alloys*. ASM International.

Appendix C: Detailed Hand Calculations for BEMT analysis

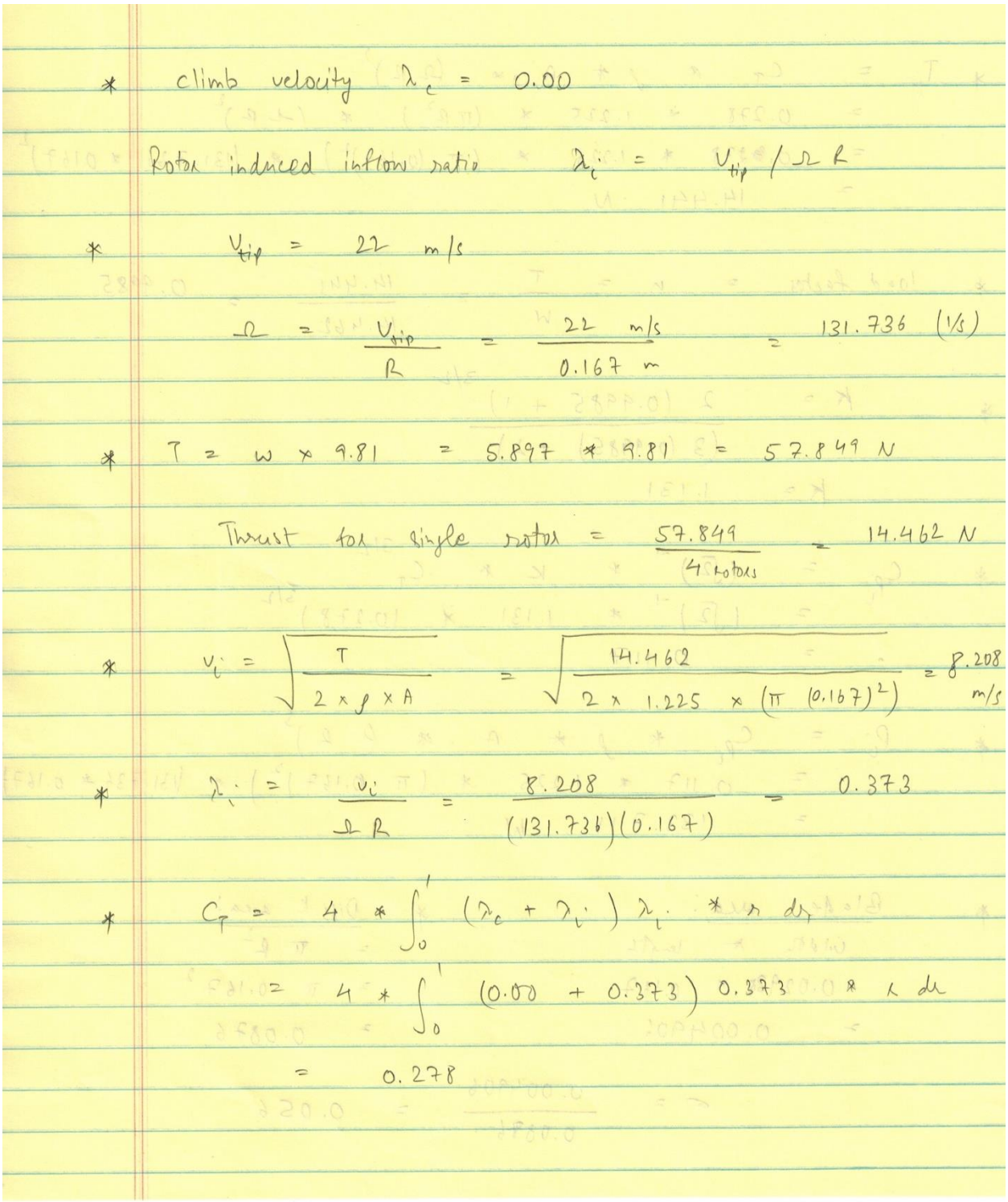

Figure 50: The calculations for rotor induced inflow ratio and coefficient of thrust

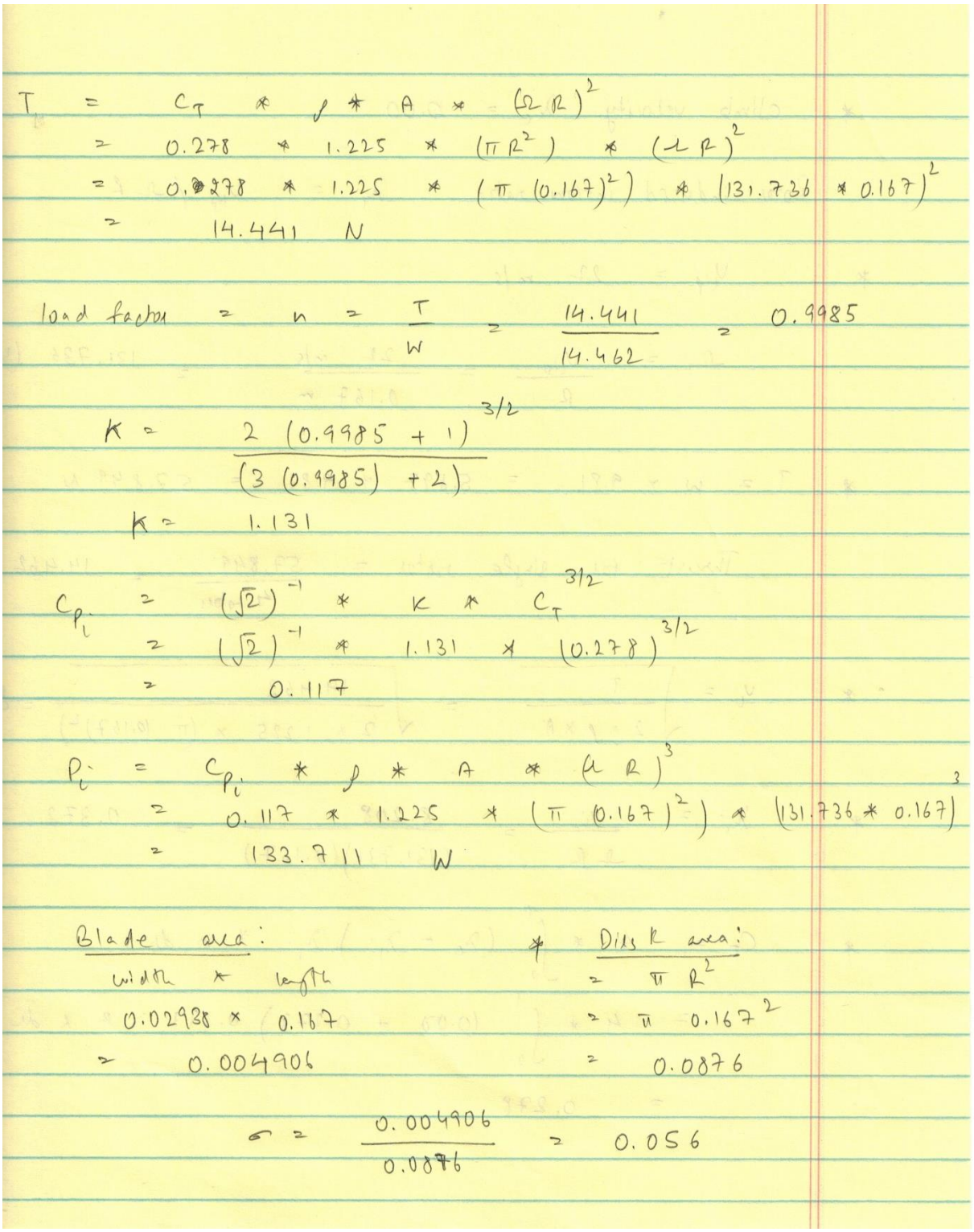

Figure 51: Show the calculations for thrust, induced power factor and induced power.

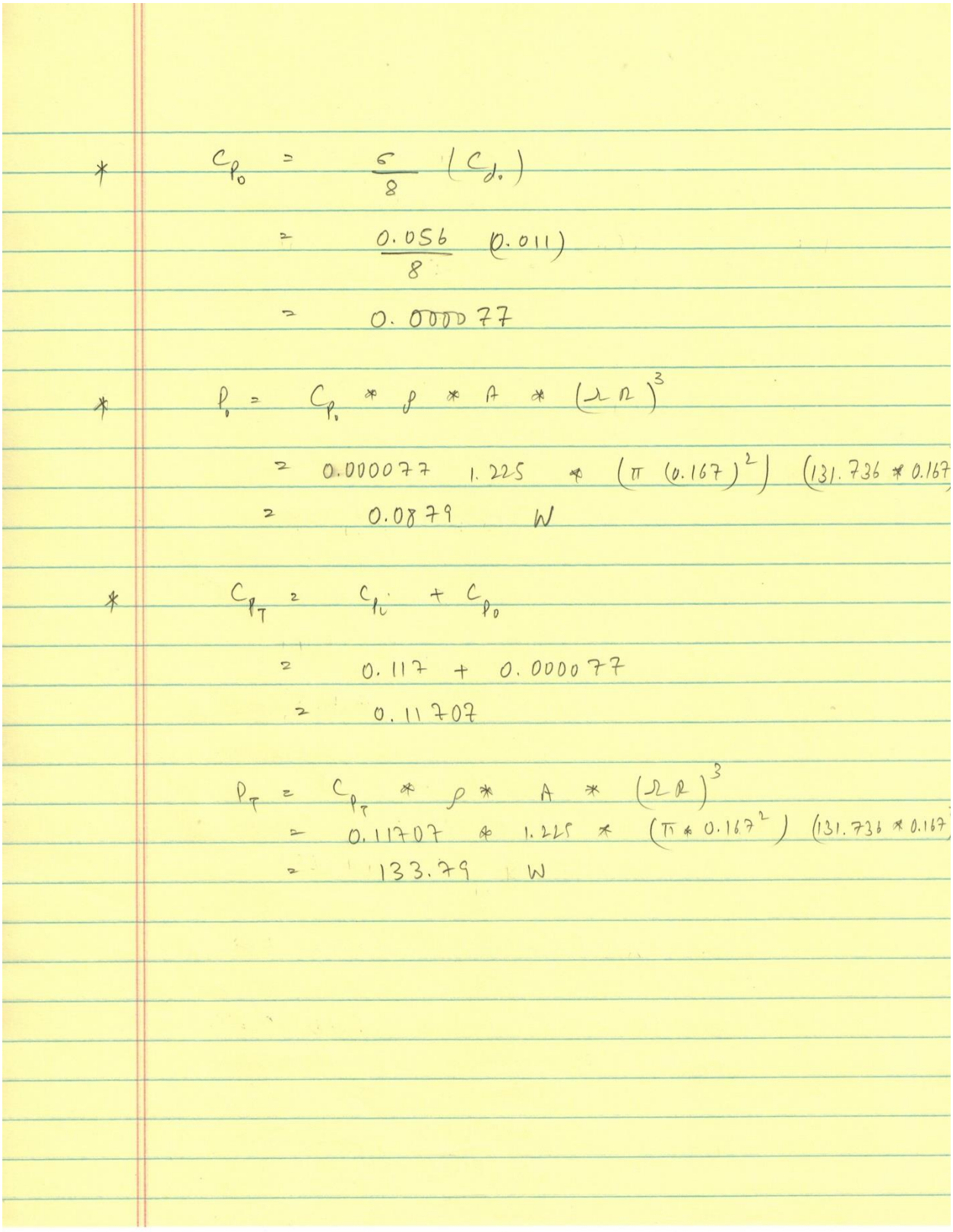

Figure 52: Show the calculations for profile power, coefficient of total power and total power.

Figure 50, Figure 51, and Figure 52 detail the calculations done for the BEMT analysis. The summary of these results can be found in Chapter 8: Detailed Analysis of SAUSER (In Hover) Using BEMT.

Appendix D: Gantt Chart

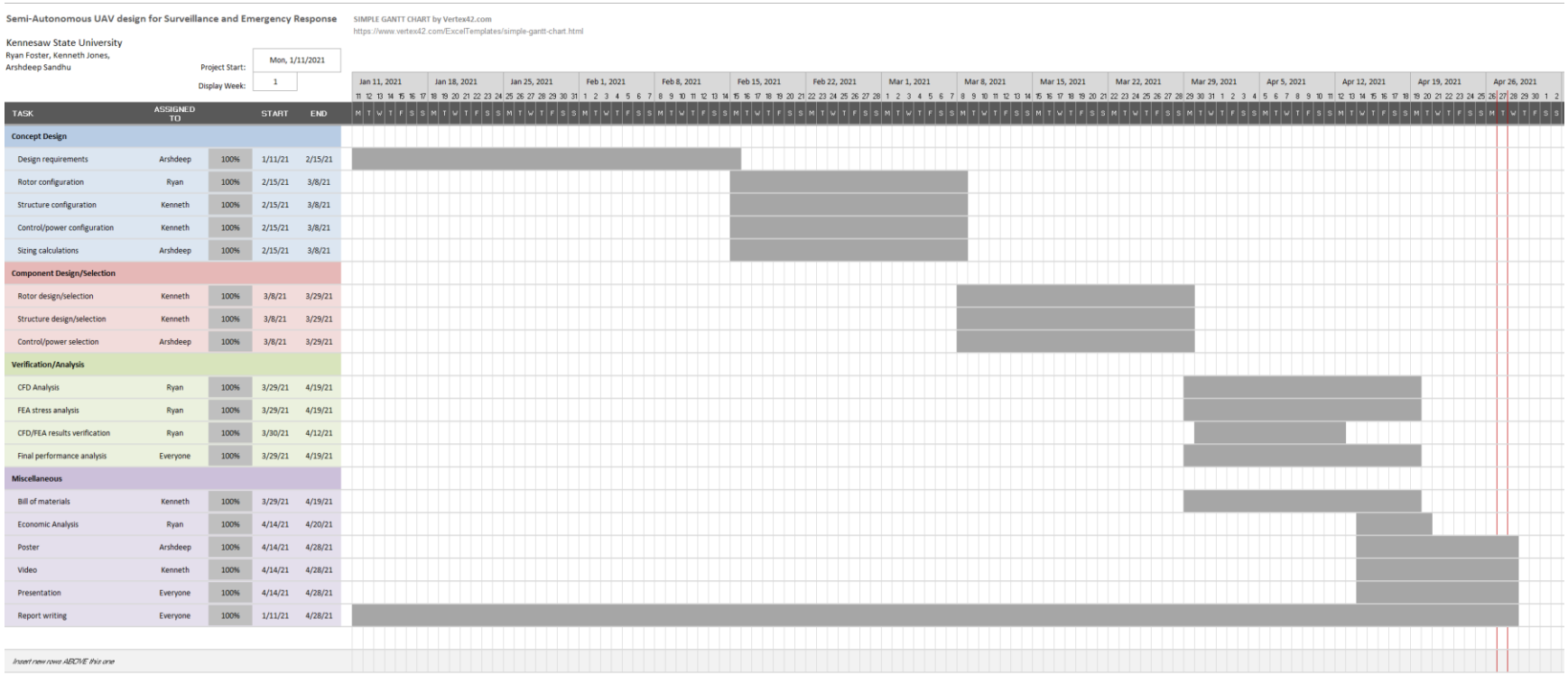

Figure 53: Gantt Chart

Figure 53: Gantt Chart is the Gantt chart used to track progress of the report. It details the division of labor throughout the course of the SAUSER project.

Appendix E: Index of Technical Contributions

Appendix E.1: Major Contributors by Chapter

Table 17 outlines the major contributors for each chapter/section of the SAUSER project.

Table 17: Major contributors by chapter

Chapter or Other Heading	**Major Contributor(s)**
Executive Summary	Ryan Foster
Chapter 1: Introduction	Kenneth Jones, Arshdeep Sandhu
Chapter 2: Literature Review	Ryan Foster
Chapter 3: Design Approach and Methodology	Kenneth Jones, Arshdeep Sandhu
Chapter 4: Concept Alternatives	Ryan Foster, Kenneth Jones
Chapter 5: Electronics	Kenneth Jones
Chapter 6: Sizing	Arshdeep Sandhu
Chapter 7: Rotor Design	Arshdeep Sandhu
Chapter 8: Detailed Analysis of SAUSER (In Hover) Using BEMT	Arshdeep Sandhu
Chapter 9: Simulations	Ryan Foster
Chapter 10: Bill of Materials	Kenneth Jones
Chapter 11: Economic Analysis	Ryan Foster, Kenneth Jones
Chapter 12: Results and Discussion	Ryan Foster, Kenneth Jones, Arshdeep Sandhu
Chapter 13: Conclusions	Ryan Foster, Kenneth Jones, Arshdeep Sandhu
Appendix A: CFD and FEA Settings	Ryan Foster
Appendix B: Manual Verification of Computational Methods	Ryan Foster
Appendix C: Detailed Hand Calculations for BEMT analysis	Arshdeep Sandhu
Appendix D: Gantt Chart	Ryan Foster, Kenneth Jones, Arshdeep Sandhu
Appendix E: Index of Technical Contributions	Ryan Foster
Appendix F: Battery Capacity Calculations	Kenneth Jones
Appendix G: CAD and Video Citations	Kenneth Jones

Note: the FDR rubric specified up to two contributors for each section. However, due to the collaborative nature of this project, several chapters had major contributions from all three team members.

Appendix E.2: Technical Contributions by Each KSU Team Member

Table 18 outlines the technical contributions by each KSU team member.

Table 18: Technical contributions by each KSU team member

Team Member	Technical Contributions
Ryan Foster	• Project management • Literature review • Concept alternatives • CFD/FEA analyses • Manual verification of CFD/FEA analyses • Economic analysis
Kenneth Jones	• Concept sketches • Concept alternatives • Electronics calculations/selections • Economic analysis • CAD design • CAD sourcing • Video editing
Arshdeep Sandhu	• Design requirements • Initial Design sketches • Literature Review • Design approach and Methodology • Sizing • Rotor design • BEMT analysis

Appendix E.3: KSU Team Member Contact Information

Ryan Foster: r.foster84@icloud.com

Kenneth Jones: Kennethkj1217@gmail.com

Arshdeep Sandhu: a96deep@gmail.com

Appendix F: Battery Capacity Calculations

Prop（inch）	Voltages（V）	Throttle (%)	Load Currency (A)	Pull(g)	Power(W)	Efficiency (g/W)	Temperature(in full throttle load 1 min)
5146	16	50%	10.27	543	164.3	3.305	68
		60%	15.28	717	244.5	2.933	
		70%	22.02	911	352.3	2.586	
		80%	29.48	1098	471.7	2.328	
		90%	38.02	1275	608.3	2.096	
		100%	47.5	1436	760.0	1.889	
6045	16	0.5	10.67	630	170.72	3.690	68
		0.6	15.82	835	253.12	3.299	
		0.7	22.63	1053	362.08	2.908	
		0.8	30.68	1266	490.88	2.579	
		0.9	39.48	1478	631.68	2.340	
		1	49.57	1649	793.12	2.079	

Figure 54: iFlight Motor information[30]

Figure 54 is the performance data of the iFlight motor used to determine the power consumption and available RPM.

[30] "XING-E 2208 2-6S FPV Motor." *IFlight*, IFlight, shop.iflight-rc.com/index.php?route=product%2Fproduct&path=20_26&product_id=881.

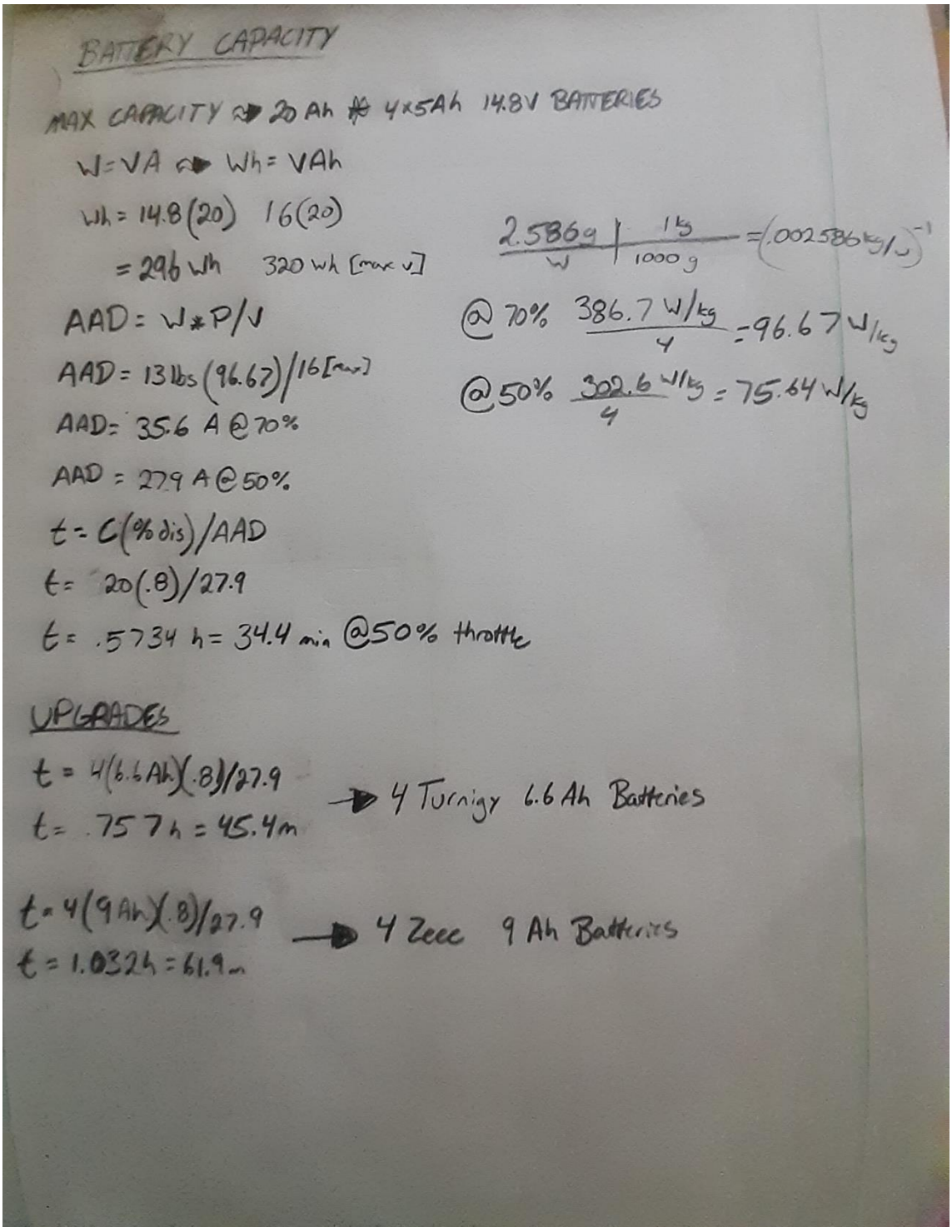

Figure 55: Battery Capacity Calculations

Figure 55 details the calculations done for the battery capacity analysis. The summary of these results can be found in Chapter 5: Electronics.

Appendix G: CAD and Video Citations

The following citations are for CAD models and other media used for the video.

From GrabCAD:

I.Fauzi. (2021, March 19th). Sports Car Design. **https://grabcad.com/library/sports-car-design-2**

L. Peaslee. (2012, October 30th). GoPro Hero 3. **https://grabcad.com/library/gopro-hero-3**

L. Wenliang. (2019, June 26th). JetsonNano. **https://grabcad.com/library/jetson-nano-3**

M. Bond. (2017, July 17th). Pixhawk. **https://grabcad.com/library/pixhawk-2**

M. Studio. (2020, February 10th). Brushless Motor 1806 2280KV. **https://grabcad.com/library/brushless-motor-1806-2280kv-1**

P. S. (2021, February 26th). Aeronaut CAM Carbon Light 13x5 Propellor. **https://grabcad.com/library/aeronaut-cam-carbon-light-13x5-propeller-1**

From Soundcloud:

AshamaluevMusic. Quickly. https://soundcloud.com/ashamaluevmusic/sets/background-music-for-presentations